universe

MDPI

Article

The Nuclear Astrophysics Program at the CERN n_TOF Facility: Results and Perspectives

P. M. Milazzo [1,2,*], C. Lederer-Woods [3] and A. Mengoni [2,4,†] on behalf of The n_TOF Collaboration

[1] Istituto Nazionale di Fisica Nucleare, Sezione di Trieste, 34149 Trieste, Italy
[2] European Organization for Nuclear Research (CERN), 1211 Geneva, Switzerland; alberto.mengoni@cern.ch
[3] School of Physics and Astronomy, University of Edinburgh, Edinburgh EH9 3FD, UK; claudia.lederer-woods@ed.ac.uk
[4] Agenzia Nazionale per le Nuove Tecnologie (ENEA), 40129 Bologna, Italy
* Correspondence: paolo.milazzo@ts.infn.it
† Membership of The n_TOF Collaboration is provided in the Appendix A.

Abstract

The CERN n_TOF facility is a research infrastructure specifically designed for studying neutron-induced nuclear reactions. Pulsed white neutron beams are delivered toward three experimental areas, two of them at different baselines to apply the time-of-flight technique, and another one very close to the neutron source for activation studies. High intensity and high neutron energy resolution make n_TOF a unique facility. A major component of the physics program at n_TOF is dedicated to the measurement of key neutron induced reactions for nuclear astrophysics, relevant to nucleosynthesis in stars, the Big Bang primordial nucleosynthesis as well as Cosmochronology. A review of the relevant results obtained at the n_TOF facility is reported, together with details of challenging new measurements in preparation.

Keywords: nuclear astrophysics; nuclear reactions; neutron physics

Academic Editors: Ragandeep Singh Sidhu, Gavin Lotay and Jaspreet Singh Randhawa

Received: 9 August 2025
Revised: 18 September 2025
Accepted: 20 September 2025
Published: 30 September 2025

Citation: Milazzo, P.M.; Lederer-Woods, C.; Mengoni, A., on behalf of The n_TOF Collaboration. The Nuclear Astrophysics Program at the CERN n_TOF Facility: Results and Perspectives. *Universe* **2025**, *11*, 329. https://doi.org/10.3390/universe11100329

1. Introduction

Neutron cross-section measurements are important in several areas of fundamental and applied nuclear physics, including nuclear astrophysics. Understanding how the chemical elements are formed is key to comprehend the evolution of the Universe. Hydrogen, Helium, and small amounts of Lithium were produced in the period between about 100 s and 20 min after the Big Bang [1–4]. This period of primordial nucleosynthesis was followed by galactic condensation and the formation of stars. Heavier elements are then formed in stars, and in particular, the production of elements from Iron to Uranium arises almost exclusively from neutron capture processes, which occur during quiescent stellar evolution or in dramatic explosive scenarios such as supernovae or neutron star mergers [5–13]. The slow neutron capture process (s-process) contributes about half of the elemental abundances between Iron and Bismuth in our solar system [14–16]. During the process, neutron densities are $n_n \lesssim 10^8$ cm^{-3} and stellar temperatures T range from 10^8–10^9 K. The nucleosynthesis path closely follows the line of stability since β-decay is generally faster than neutron capture. The main component of the s-process, producing mainly isotopes between Zr and Bi, occurs in the Asymptotic Giant Branch (AGB) phase of low mass stars ($M < 8M_\odot$) [17,18], after He core burning is exhausted and H- and He burning continues in shells around an inert C/O core. The weak component of the s-process takes place in massive stars ($M \gtrsim 8$–$10\ M_\odot$) during He core and C shell burning

phases and contributes mainly to elemental abundances from Fe to Zr [19,20]. The weak s-process component should be considered as the direct product of the activation of the ^{22}Ne(α, n)^{25}Mg reaction as a source of free neutrons.

In contrast, the rapid neutron capture process (r-process) takes place in stellar explosions at neutron densities $n_n > 10^{20}$ cm^{-3} and temperatures $T > 10^9$ K. Neutron capture reactions occur fast, and the reaction path proceeds far from stability involving short-lived, exotic nuclei.

A number of metal-poor stars show an abundance pattern that cannot be explained by the s- or the r-process. Their peculiar abundance pattern may be explained by an intermediate neutron capture process (i-process) [21], with neutron concentrations intermediate between the s- and r-processes ($n_n \approx 10^{12}$–10^{16} cm^{-3}).

A progress in the quantitative description of the neutron-capture processes can be achieved by an interdisciplinary approach involving improved nuclear physics input, stellar models, observations of stellar spectra, and isotopic analysis of meteorites. Relevant advances in stellar evolutionary codes, taking into account additional physics aspects, e.g., the role played by magnetic fields [22], and new high-quality data from astronomical observations need to be complemented by high precision measurement of neutron-induced reactions, with target uncertainties of 5% or lower. The neutron beam delivered at the n_TOF facility is well tailored to fully cover the neutron spectrum up to ~500 keV, the stellar energy range of interest for the different nucleosynthesis processes considered.

This article will present the nuclear astrophysics program at the CERN n_TOF facility since its inception and the impact results have made on nuclear astrophysics research and will mention the planned improvements of the facility. The list of performed measurements, dedicated to several aspects of nuclear astrophysics, is reported in Tables 1 and 2.

Table 1. List of isotopes relevant for nuclear astrophysics for which (n, γ) measurements have been performed at n_TOF since its inception.

Isotope	Astrophysical Implications	Measured Energy Range	Detectors Used	Ref.
^{24}Mg	Impact on abundance of cosmic gamma ray emitter ^{26}Al	0–700 keV	C_6D_6	[23]
^{25}Mg	Constraints for the ^{22}Ne(α, n), neutron poison	0–550 keV	C_6D_6	[23]
^{26}Mg	Neutron poison	0–500 keV	C_6D_6	[23,24]
^{28}Si	Isotopic abundances in presolar grains, nucleosynthesis in massive stars	Under Analysis	C_6D_6, STED	[25]
^{29}Si	Isotopic abundances in presolar grains, nucleosynthesis in massive stars	Under Analysis	C_6D_6, STED	[25]
^{30}Si	Isotopic abundances in presolar grains, nucleosynthesis in massive stars	Under Analysis	C_6D_6, STED	[25]
^{40}Ar	Nucleosynthesis processes involving noble gases	Under Analysis	C_6D_6, STED	[26]
^{54}Fe	Seeds of the s-process nucleosynthesis path	0–400 keV	C_6D_6	[27]
^{57}Fe	Seeds of the s-process nucleosynthesis path	0–400 keV	C_6D_6	[27]
^{58}Ni	s-process nucleosynthesis in massive stars	0–400 keV	C_6D_6	[28]
^{62}Ni	s-process nucleosynthesis in massive stars	0–200 keV	C_6D_6	[29]
^{63}Ni	Branching point	0–270 keV	C_6D_6	[29,30]
^{64}Ni	s-process nucleosynthesis in massive stars	Under Analysis	C_6D_6	[31]
^{70}Ge	s-Only isotope, test for s-process nucleosynthesis	0–300 keV	C_6D_6	[32]
^{72}Ge	s-process nucleosynthesis in massive stars	0–300 keV	C_6D_6	[33]
^{73}Ge	s-process nucleosynthesis in massive stars	0–300 keV	C_6D_6	[34]
^{74}Ge	s-process nucleosynthesis in massive stars	0–70 keV	C_6D_6	[35]
^{76}Ge	s-process nucleosynthesis in massive stars	0–52 keV	C_6D_6	[36]
^{77}Se	s-process nucleosynthesis in massive stars	0–51 keV	C_6D_6	[37]
^{78}Se	s-process nucleosynthesis in massive stars	0–70 keV	C_6D_6	[38]
^{79}Se	Branching point	Under Analysis	STED	[39]

Table 1. *Cont.*

Isotope	Astrophysical Implications	Measured Energy Range	Detectors Used	Ref.
^{80}Se	s-process nucleosynthesis in massive stars	0–70 keV	C_6D_6	[40]
^{87}Sr	^{87}Rb/^{87}Sr cosmochronometer	Under Analysis	C_6D_6, STED	[41]
^{89}Y	Bottleneck around N = 50	0–95 keV	C_6D_6	[42]
^{90}Zr	Bottleneck at N = 50	0–70 keV	C_6D_6	[43]
^{91}Zr	Bottleneck at N = 50	0–26 keV	C_6D_6	[44]
^{92}Zr	Bottleneck at N = 50	0–81 keV	C_6D_6	[45,46]
^{93}Zr	Bottleneck at N = 50	0–8 keV	C_6D_6	[47]
^{94}Zr	Bottleneck at N = 50	0–60 keV	C_6D_6	[48]
^{96}Zr	Branching at ^{95}Zr	0–40 keV	C_6D_6	[49]
^{94}Nb	Branching point	Under Analysis	C_6D_6, STED	[50]
^{92}Mo	Disentangling s-, r-, p-process contributions to Mo isotopes	Under Analysis	C_6D_6, STED	[51]
^{94}Mo	Mo abundances in presolar grains	Under Analysis	C_6D_6, STED	[52]
^{95}Mo	s-process nucleosynthesis in AGB stars	Under Analysis	C_6D_6, STED	[52]
^{96}Mo	Disentangling s-, r-, p-process contributions to Mo isotopes	Under Analysis	C_6D_6, STED	[51]
^{97}Mo	Disentangling s-, r-, p-process contributions to Mo isotopes	Under Analysis	C_6D_6, STED	[51]
^{98}Mo	Disentangling s-, r-, p-process contributions to Mo isotopes	Under Analysis	C_6D_6, STED	[51]
^{100}Mo	Disentangling s-, r-, p-process contributions to Mo isotopes	Under Analysis	C_6D_6, STED	[51]
^{121}Sb	Constraints on the s-nucleosynthesis path	Under Analysis	C_6D_6	[53]
^{122}Sb	Constraints on the s-nucleosynthesis path	Under Analysis	C_6D_6	[53]
^{139}La	Bottleneck at N = 82	0–9 keV	C_6D_6	[54]
^{140}Ce	Bottleneck around N = 82	0–65 keV	C_6D_6	[55,56]
^{146}Nd	s-process nucleosynthesis in AGB stars	Under Analysis	STED	[57]
^{151}Sm	Branching point	0–1 MeV	C_6D_6	[58,59]
^{154}Gd	s-only isotope, test for s-process nucleosynthesis	0–300 keV	C_6D_6	[60]
^{160}Gd	s-process nucleosynthesis in AGB stars	Under Analysis	C_6D_6	[61]
^{164}Er	s-only isotope, test for s-process nucleosynthesis	Under Analysis	C_6D_6	[62]
^{171}Tm	Branching point	0–1 keV	C_6D_6	[63]
^{176}Yb	s-process nucleosynthesis in AGB stars	0–21 keV	C_6D_6	[64]
^{186}Os	^{187}Re/^{187}Os cosmochronometer	0–1 MeV	C_6D_6	[65,66]
^{187}Os	^{187}Re/^{187}Os cosmochronometer	0–1 MeV	C_6D_6	[65,66]
^{188}Os	^{187}Re/^{187}Os cosmochronometer	0–1 MeV	C_6D_6	[65,66]
^{197}Au	Standard (n, γ) cross section	0–400 keV	C_6D_6, TAC	[67,68]
^{204}Tl	Branching point	0–1 keV	C_6D_6	[69]
^{205}Tl	Part of branching point at A = 204	0–100 keV	C_6D_6	[70]
^{204}Pb	Termination of s-nucleosynthesis path	0–440 keV	C_6D_6	[71]
^{206}Pb	Termination of s-nucleosynthesis path	0–620 keV	C_6D_6	[72]
^{207}Pb	Termination of s-nucleosynthesis path	3–320 keV	C_6D_6	[73]
^{209}Bi	Termination of s-nucleosynthesis path	0–23 keV	C_6D_6	[74]

Table 2. List of isotopes relevant for nuclear astrophysics for which (n, p) and (n, α) measurements have been performed at n_TOF since its inception. Measurements were performed by means of solid-state silicon detectors.

Isotope	Astrophysical Implications	Measured Energy Range	Ref.
(n, p) reactions			
^{7}Be	Cosmological Lithium Problem	0–325 keV	[75]
^{14}N	Neutron poison	0–800 keV	[76]

Table 2. *Cont.*

Isotope	Astrophysical Implications	Measured Energy Range	Ref.
^{26}Al	Cosmic γ-ray emitter	0–150 keV >150 keV Under Analysis	[77]
^{40}K (n, α) reactions	Radiogenic heating of Earth-like exoplanets	Under Analysis	[78]
^{7}Be	Cosmological Lithium Problem	0–10 keV	[79]
^{26}Al	Cosmic γ-ray emitter	0–150 keV >150 keV Under Analysis	[80]
^{40}K	Radiogenic heating of Earth-like exoplanets	Under Analysis	[78]
^{41}Ca	Short-lived radionuclei in Early Solar System	Under Analysis	[81]

2. The n_TOF Facility

The neutron time-of-flight facility n_TOF is a neutron source that has been operating at CERN since 2001 [82,83]. Neutrons are produced by spallation reactions of a 20 GeV/c pulsed proton beam hitting a massive lead block. With a conversion ratio of about 300 neutrons per proton, each beam pulse consisting today of 8.5×10^{12} protons yields a neutron flux of 2×10^{15} neutrons per pulse. This high instantaneous neutron flux leads to excellent suppression of backgrounds unrelated to the neutron beam, such as sample radioactivity [84,85].

Charged particles are removed from the neutron beam by sweeping magnets, and neutrons and ultra-relativistic particles outside the beamlines are suppressed by heavy concrete walls and a massive iron shielding. Water moderators shape the initially fast neutron spectrum into wide energy fields, spanning over 12 orders of magnitude, from meV up to the GeV range, with a nearly $1/E$ isolethargic flux dependence up to 1 MeV. As shown in Figures 1 and 2, neutrons are delivered through vacuum pipelines to three experimental areas (EAR): EAR1 at ≈185 m, EAR2 at ≈20 m, and the near EAR (NEAR) at ≈3 m distance from the spallation target. The collimation process provides a nearly symmetric Gaussian-shaped beam profile at the sample position.

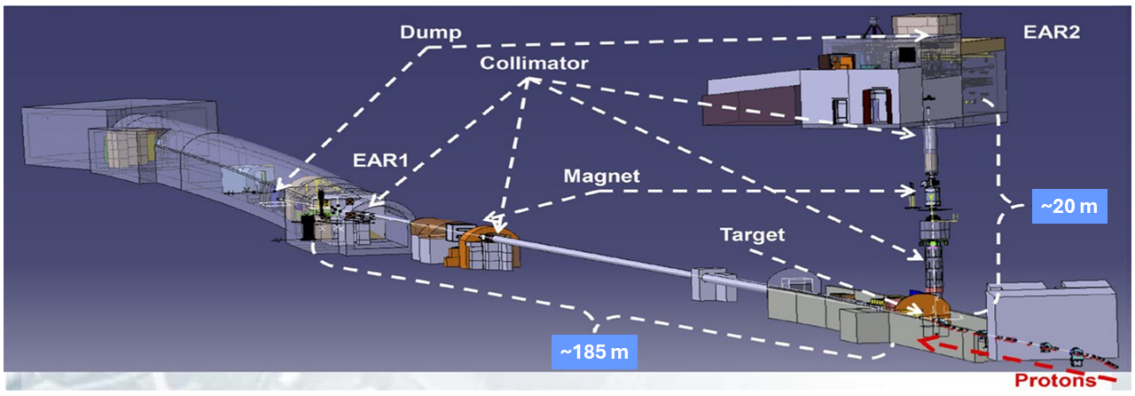

Figure 1. Layout of the CERN n_TOF facility, including details of EAR1 and EAR2 flight path.

The EAR1 and EAR2 experimental areas are dedicated to neutron cross-section measurements using the time-of-flight technique, where the kinetic neutron energy E_n for each capture event is deduced by measuring the time between production of the neutron and neutron-induced reaction. The long flight paths lead to excellent neutron energy resolution, in particular in EAR1; a short proton pulse width of 7 ns RMS enables a resolution from 0.03% at 1 eV to 0.3% at 100 keV. While the shorter flight path at EAR2 reduces the available neutron

energy resolution, the higher neutron flux makes it particularly well suited for measurements on small and/or radioactive samples, even when the mass of the sample is just a few mg. The NEAR experimental area is mainly used for neutron activation measurements, where an energy-integrated cross section is measured by irradiation and subsequent radioactive decay counting [86]. In this area, a typical neutron flux up to 10^{13} n/cm^2/year is available.

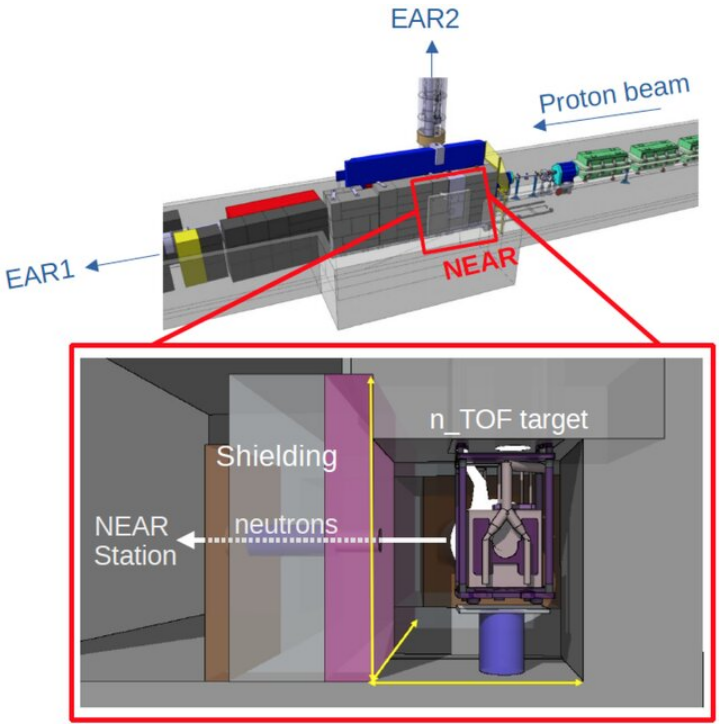

Figure 2. A scheme of the NEAR station. The bottom part in the red box shows an upstream view with respect to the beam direction.

The combination of these features makes n_TOF a unique facility, allowing for performing measurements with unprecedented accuracy and resolution on stable isotopes, as well as for investigating neutron-induced reactions on short-lived unstable nuclei.

3. Experimental Setups

This section describes the detection setups used today for measurements of astrophysical interest, in particular γ-ray detectors and solid-state detectors.

3.1. C_6D_6 Liquid Scintillators

Deuterated benzene C_6D_6 liquid scintillators have been used successfully for several decades to measure radiative capture cross section. They are insensitive to scattered neutrons, which is one of the most important background components in this type of measurements, and have a fast response time in the ns range. The n_TOF setup has been developed in-house to minimize neutron sensitivity [87,88]. The C_6D_6 liquid (of about 1 L volume) is contained in a cylindrical low mass carbon fiber housing. The low neutron capture cross sections of both carbon and deuterium ensure a low contribution from sample scattered neutrons to the background. The design is based on detailed Monte Carlo simulations of all detector components and reduction of materials to the smallest possible level around the scintillator cells. This enables measurements on nuclei with small capture cross sections (e.g., magic nuclei) and/or nuclei with high scattering to capture ratios. A set of these detectors around the sample position in EAR1, where they are typically used, is shown in Figure 3.

The detectors detect at most one γ-ray per capture cascade, and the detection efficiency is accounted for by employing the Total Energy Detection technique [89]. To detect capture events independent of the cascade multiplicity, the intrinsic efficiency of detectors has to be corrected such that it is linearly increasing with γ-ray energy. The required proportionality is achieved via the Pulse Height Weighting Technique, an off-line modification of the response function of the detector [90,91].

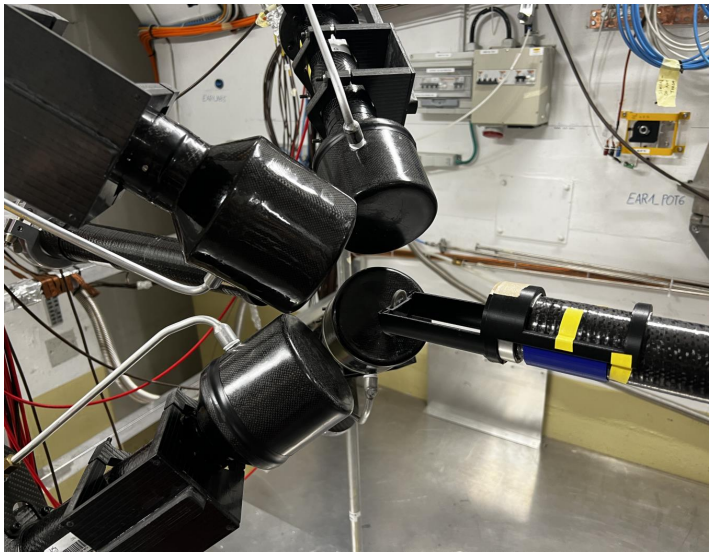

Figure 3. A set of C_6D_6 liquid scintillators around the sample position at EAR1.

3.2. The Segmented Total Energy Detector

The high instantaneous neutron flux at EAR2 results in high counting rates in above-mentioned carbon-fiber housed C_6D_6 detectors, causing pile-up effects, high dead time corrections, and gain shifts. This motivated the development of the Segmented Total Energy Detector (sTED), consisting of an array of small volume C_6D_6 modules [92] (see Figure 4). Each sTED module has an active volume of 0.044 L, which is about 23 times smaller than the active volumes of C_6D_6 detectors. Neutron capture cross-section measurements up to 400 keV neutron energy have been successfully performed with this setup.

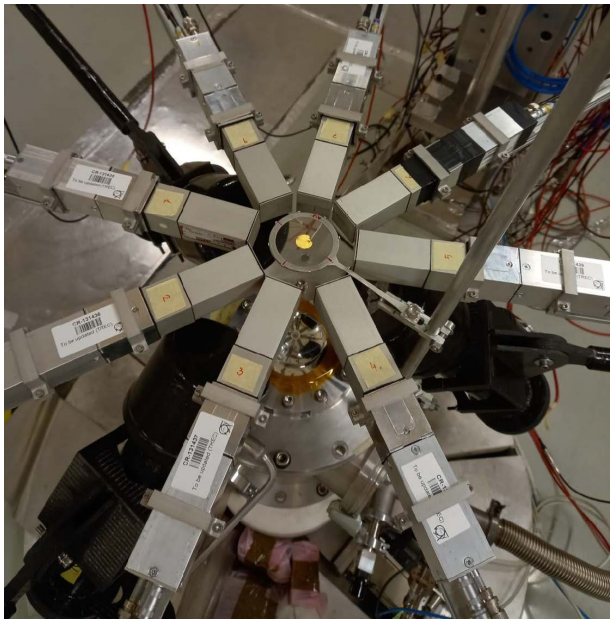

Figure 4. The sTED array consisting of eight modules.

3.3. The Total Absorption Calorimeter

The total absorption calorimeter (TAC) is installed at EAR1 and consists of 40 BaF_2 crystals arranged in almost 4π geometry (see Figure 5), resulting in a capture detection efficiency of close to 100%. The crystals are contained in ^{10}B loaded carbon fiber capsules, coupled to XP4512B photomultipliers and purpose designed voltage dividers. Since this setup has higher neutron sensitivity compared with the C_6D_6-type detectors, the samples are surrounded by a neutron absorber, which moderates and absorbs sample scattered neutrons. The calorimeter can be used to select the γ-ray cascade from neutron capture using total deposited energy and therefore can be used to suppress background due to γ-rays originating from other processes [93].

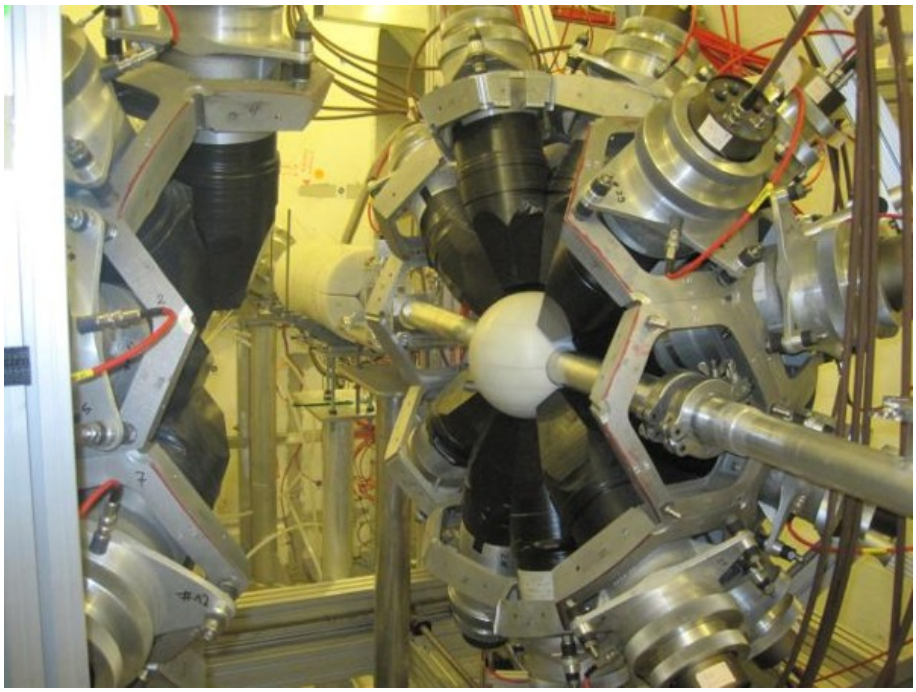

Figure 5. The total absorption calorimeter. The two hemispheres are closed during measurements.

3.4. Solid-State Detectors

While most neutron-induced reactions relevant in nuclear astrophysics are radiative capture reactions, there are a number of reactions producing light charged particle reactions. Several detection setups consisting of silicon strip detectors have been developed for this purpose. For the detection of outgoing charged particles, the ΔE-E technique has been used when possible, allowing particle identification. These setups are described in more detail in Sections 8 and 10.

4. The Relevant Role of Neutron Capture Cross Sections Along the Nucleosynthesis Path

The abundances produced in the nucleosynthesis processes are essentially determined by the neutron capture cross sections of the involved isotopes. The stellar neutron capture rate can be defined as the neutron capture cross section $\sigma(E_n)$ integrated over the neutron velocity distribution, $\langle \sigma v \rangle = \int_0^\infty \sigma v \Phi(v) dv$. The velocity distribution $\Phi(v)$ of the neutron flux is described by a Maxwell–Boltzmann form [94], because neutrons are quickly thermalized in the He burning stellar plasma, where the nucleosynthesis process takes place.

For a given isotope of mass A, the term $\langle \sigma v \rangle$ can be expressed as $\sigma_A v_T$ by introducing the Maxwellian-averaged capture cross section (MACS) σ_A for the isotope of mass A and

the mean thermal neutron velocity v_T. Once the neutron capture cross sections are known for all relevant energies, MACS can be calculated for different stellar temperatures T to take into account the different stellar scenarios.

However, experimental data alone are not sufficient for a full definition of the reaction rate. In fact, in a stellar environment, the high s-process temperatures imply that nuclei might be excited by the intense and energetic thermal photon bath. For nuclei with excited states at low energies (say, $<$100 keV), this may result in a significant thermal population of the low-lying levels. From experiments, we have only the cross section for nuclei in their ground state, which represent only a part of the information required to derive the stellar rate. To recover the missing information, an estimation of the so-called Stellar Enhanced factor (SEF), i.e., the ratio between MACS at stellar environments and at ground state, can be calculated from theory [95].

In addition, one should consider that the ground-state MACS can be calculated by folding the capture cross section with the respective thermal neutron spectrum at the s-process site. To cover all possible thermal energy ranges, cross-section data should be available over a sufficiently wide neutron energy range, starting at about 100 eV and extending to about 500 keV to account for the highest temperatures reached during shell carbon burning in massive stars. In some instances, the energy range accessible via direct experimental measurements is limited to the "resolved resonance region", which could be limited in the higher energy range. To complement for the missed neutron energy range, it is necessary to adopt a theoretical modeling of the capture reaction process. The use of cross sections from evaluated data libraries can be adopted in most cases.

MACSs are the main player in driving the s-process nucleosynthesis path including the particular feature of so-called critical points. The following are the two kinds of these critical points:

1. The relatively small neutron capture cross section of nuclides with neutron magic numbers plays a crucial role along the nucleosynthesis path because they act as bottlenecks. The abundance N_A of a stable isotope of mass A is determined by the respective rates for production and destruction, as follows:

$$\frac{dN_A}{dt} = -\sigma_A \cdot N_A + \sigma_{A-1} \cdot N_{A-1}.$$

   In a steady-state situation (typical of the s-process) with $dN_A/dt = 0$, the product $\sigma_A \cdot N_A$ is constant for all A. Indeed, the $\sigma_A \cdot N_A$ distribution appears roughly constant in mass regions between magic neutron numbers (50, 82, 126), thus indicating that assumed flow equilibrium is at least partly reached. On the contrary, the very small neutron capture cross sections of neutron magic isotopes limit the reaction flow and give rise to structures in the $\sigma_A \cdot N_A$ distribution. As a consequence, three main peaks are present in the elemental abundance distribution close to neutron magic numbers.
2. The branchings on the s-process path occurs due to unstable isotopes with a relatively long half-life ($t_{1/2}$) larger than about a year. The neutron capture process can proceed or not through these isotopes strictly depending on the stellar conditions (temperature and neutron density).

These isotopes provide unique tracers and allow for a deep investigation of the star physical conditions and complicated details of stellar nucleosynthesis. Neutron-capture measurements on these isotopes, in combination with stellar spectroscopy and isotopic analyses of primitive meteorites, can help to better understand the role of stellar mass, rotation, or metallicity; to constrain the properties of non-convective mixing in stellar interiors; and to refine our understanding of galactic chemical evolution. Measurements of isotopes belonging to these two groups are detailed in the next two sections.

5. Bottlenecks Along the Nucleosynthesis Path

5.1. The Nucleosynthesis Path Around the Neutron Magic Number N = 50

The first s-process peak is located around Sr, Y, and Zr that have isotopes with N $\sim$ 50. Neutron capture cross sections on N = 50 nuclides are small, and thus strongly influence the production of all heavier elements (at least) up to the second s-process peak, around the neutron magic number of 82 (the third peak is represented by Pb and Bi, near N = 126). In addition, the $A = 90$ region represents a border between different components of the s-process, the main one responsible for the production of elements with $A > 90$ and the weak one dominantly responsible for abundances of elements with $A < 90$. The neutron capture on ^{89}Y, all the stable Zr isotopes, and the unstable ^{93}Zr has been investigated at EAR1 of n_TOF [43–49]. The neutron magic nucleus ^{90}Zr and the stable isotopes ^{91}Zr, ^{92}Zr, and ^{94}Zr are all predominantly of s-process origin. As far as the unstable isotopes ^{93}Zr and ^{95}Zr are concerned, the first one can be considered as stable on the time scale of the s-process because of its long half-life of $\approx$1.5 Myr. In contrast, ^{95}Zr represents a true branching point, where the reaction flow splits. The short half-life of ^{95}Zr ($t_{1/2}$ = 64 days) prevents a large part of the reaction flow from reaching ^{96}Zr. On the other hand, during thermal pulses in AGB stars, neutron densities produced by ^{22}Ne(α, n) reactions can reach 10^{11}–10^{12} cm^{-3}, sufficient to produce ^{96}Zr. However, ^{96}Zr is destroyed by neutron capture during the hydrogen shell burning phases where neutron densities from the ^{13}C(α, n) neutron source are too small to produce ^{96}Zr.

While the isotopic ratios of most elements can only be inferred from terrestrial material, which represents an average of many sources, Zr isotope ratios can also be determined for individual sources, either by analyses of microscopic dust grains of presolar origin or by spectroscopy of the band structure of ZrO in cool AGB stars [96]. Presolar grains can be recovered from primitive meteorites. Laboratory analyses of these µm-sized grains have revealed isotopic patterns completely different from those of the bulk of solar system material. Since isotopic compositions can only be modified by nuclear reactions, stardust grains carry the signature of their formation environments around different types of astrophysical objects, from giant stars to novae and supernovae. The cross section obtained at n_TOF have been used to calculate isotopic ratios of different Zr isotopes produced in stars, and improved agreement between stellar models and measured isotopic ratios of grains has been reached [97].

5.2. The Nucleosynthesis Path Around the Neutron Magic Number N = 82

The second s-process peak is shaped by the neutron magic N = 82 nuclei from Ba to Nd, and their cross sections determine the s-process abundances from Ba up to Pb. Several isotopes belonging to this region have also been investigated at n_TOF.

5.2.1. $^{139}La(n,\gamma)$

High-accuracy cross section on the most abundant isotope of Lanthanum, ^{139}La, has been obtained at n_TOF [54]. This included neutron resonance parameters and MACS at s-process temperatures between $kT = 8$ and 30 keV. Lanthanum isotopic abundances can be measured at stellar spectra with good accuracy; hence, accurate cross sections are key to compare stellar model predictions to measured ones in different types of stars. In particular, transition probabilities and hyperfine structure constants of several ^{139}La levels have been accurately measured in stellar absorption spectra, and its abundance can be determined in stars of different metallicities [98]. These analyses of abundances depend sensitively on the MACS at the typical temperatures of the astrophysical site of the main s-process. Resonance parameters have been determined with high accuracy and show differences

with respect to the previous experimental data; related nuclear quantities have then been extracted with improved accuracy.

5.2.2. $^{140}Ce(n,\gamma)$

For a long time, model predictions have been in disagreement with astrophysical observations of abundances of ^{140}Ce in some low-mass (<2M$_\odot$), low-metallicity globular cluster stars (present in the galactic disk), while all neighboring isotopes (Ba, La, Pr, and Nd) are well described [99]. Cerium abundances are derived from high-resolution spectra, characterized by extremely small observational errors. Given this puzzling situation, a high-accuracy measurement was proposed and performed at n_TOF in order to investigate if this disagreement might be ascribed to an overestimation of the ^{140}Ce MACS at stellar temperatures, corresponding to kT from 8 to 35 keV [55,56]. An unprecedented combination of a high-purity sample (enriched in ^{140}Ce to 99.4%) and low neutron sensitivity of in-house developed C_6D_6 detectors was set up. The obtained MACS is surprisingly 40% higher than previously accepted values [100], while stellar model calculations asked for a reduction around 20% of the s-process contribution. The n_TOF results, going in the opposite direction, thus even worsened the disagreement between predictions and observations, questioning the reliability of spectroscopic abundances or, eventually, pointing to the presence of the i-process contributing to shape the observed stellar surface distributions.

5.3. The Nucleosynthesis Path Around the Neutron Magic Number N = 126 and the End of the s-Process Nucleosynthesis

Pb isotopes and ^{209}Bi are the heaviest isotopes produced by the s-process, and they are mostly produced in low-metallicity AGB stars. In particular, Bi is the last element synthesized, further neutron captures on this isotope are recycled back to ^{206,207,208}Pb via α-decays (see also Figure 6). Relative abundances of different Pb isotopes depend on T and n_n of the stellar site because of the presence of branching points in Hg and Tl, and an accurate knowledge of all relevant MACSs allows for discriminating different stellar conditions. In addition, an accurate determination of Pb and Bi abundances produced in the s-process allows for disentangling the s-process contribution from radiogenic production (by decays from actinides produced by the r-process). Neutron captures on ^{206}Pb, ^{207}Pb, ^{208}Pb, and ^{209}Bi have been measured at n_TOF EAR1, and high accuracy results have been discussed for their astrophysical implications in several papers [72–74].

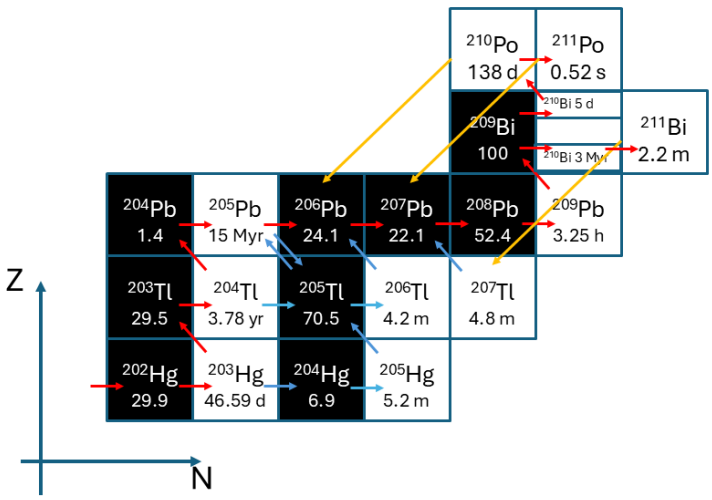

Figure 6. Schematic chart of nuclei at the termination of the s-process. Red arrows correspond to the main s-process path, while the blue ones indicate a path only enhanced during high temperature and high neutron density events. Orange arrows refer to α decays.

6. Branching Points

Radioactive isotopes along the s-process nucleosynthesis path can act as branching points, where neutron capture and β-decay compete. The abundances of the nuclei in the vicinity of a branching point depends strongly on the individual cross sections, neutron density of the star, and—in case the half-life of the branching point is temperature dependent—stellar temperature. Hence, if the s-process abundances affected by a branching point are known (for example, for s-only isotopes), knowledge of the cross sections can provide information on stellar neutron densities and/or stellar temperatures, thus helping in identifying the mass of the progenitor. The radioactivity of samples corresponding to branching points makes them particularly challenging to measure, as usually, only very small amounts of sample material can be obtained. In addition, for radiative neutron capture experiments, the capture cascade γ-rays need to be separated from any γ-rays from radioactive decay. The high instantaneous neutron flux achieved at n_TOF experimental areas makes it one of the best-suited facilities in the world for measuring radioactive samples. In fact, higher fluxes can compensate when a minor amount of sample mass is available [39]. The time in which the n_TOF detection system acquires signals is only a fraction of a second (<100 ms), and this fact improves the signal-to-radiative-noise ratio.

A list of the most relevant branching points in the s-process can be found in Table III of Ref [11]. As reported in the recent review article [101], several of the isotopes listed there have been successfully measured (often for the first time) at the n_TOF facility. The following subsections briefly describe each case.

6.1. $^{63}Ni(n, \gamma)$

As already mentioned, abundances between Fe and Zr are mainly produced by the weak s-process component in massive stars. At the end of He core burning, the neutron source ^{22}Ne(α, n)^{25}Mg is activated at temperatures around 0.3 GK, with neutron densities of $n_n \approx 10^7$ cm^{-3}. Due to such low n$_n$, more than 90% of ^{63}Ni (terrestrial $t_{1/2}$ = 101 yr) β-decays to ^{63}Cu. During the later C shell burning phase, temperatures rise to about 1 GK, and the neutron densities reached are orders of magnitude higher, n$_n \approx 10^{11-12}$ cm^{-3}. Although the stellar ^{63}Ni half-life reduces to a few years at these high stellar temperatures, ^{63}Ni behaves like a stable isotope due to the high neutron densities. ^{64}Ni is produced by ^{63}Ni(n, γ) reactions, and ^{63}Cu abundances from this later burning phase come from radiogenic decay of the accumulated ^{63}Ni. Hence, the abundances of ^{64}Ni and the two stable Cu isotopes ^{63,65}Cu sensitively depend on ^{63}Ni neutron capture cross sections [102]. The nucleosynthesis path in the Ni–Cu–Zn region is shown in Figure 7.

The neutron capture cross section on ^{63}Ni has been measured for the first time at stellar neutron energies at EAR1 [30]. The ^{63}Ni sample used in the measurement was produced already in the 1980s by bombarding enriched ^{62}Ni at a high-flux reactor at the Institute Laue–Langevin (ILL) in Grenoble (France) [103], yielding an enrichment of about 10% in ^{63}Ni, corresponding to a mass of about 110 mg. The energies and strengths of 12 new resonances for E$_n \lesssim$ 200 keV were obtained, which allowed for obtaining MACS over the entire energy range of interest, from kT = 5 to 100 keV. Stellar models of massive star nucleosynthesis using the new MACS predicted higher abundances by about 20% for ^{64}Ni, while ^{63}Cu is depleted by about 15% with respect to previous predictions.

The measurement was complemented with the measurement of the neutron capture cross section on stable ^{62}Ni for a reliable evaluation of this dominant background component in the data [29].

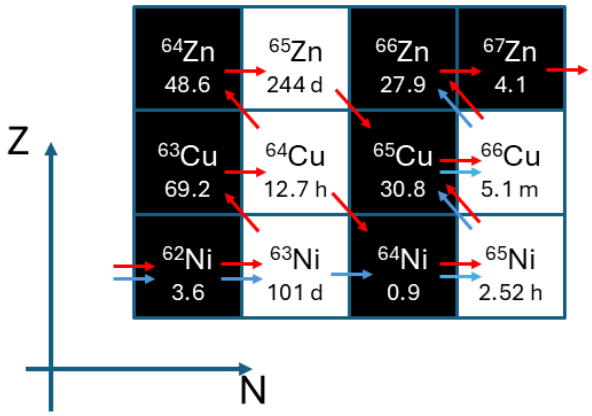

Figure 7. Schematic chart of nuclei in the Ni–Cu–Zn region. Red arrows correspond to the s-process path during He core burning, while the blue ones indicate the s-process path in the later C shell burning phase, where neutron densities are orders of magnitude higher.

6.2. $^{79}Se(n, \gamma)$

The capture cross section of ^{79}Se, never measured before, determines the reaction flow of the s-process in the Se–Br–Kr region. This key quantity fixes the relative abundance of the s-only isotopes ^{80}Kr and ^{82}Kr. Their abundance ratio is well characterized in presolar grains, and reliable constraints for the s-process site conditions can be investigated from it, in particular considering that the ^{79}Se half-life is very sensitive to the stellar temperature [104].

The main obstacle in the past to perform this measurement was the limitation in the available sample mass and detection sensitivity, given the terrestrial half-life of 3.25×10^5 years. The sample used in the measurement contained only 3 mg of ^{79}Se, the rest being a total of about 4 g of Pb, Al, and ^{78}Se. It was obtained by irradiating PbSe (Lead selenide) at ILL and inserted into an aluminum case. Although the ^{78}Se(n, γ)^{79}Se reaction in PbSe produced only a tiny amount of ^{79}Se, it could be studied for the first time at n_TOF [39].

The data at n_TOF have been taken in both experimental areas EAR1 and EAR2, with an ancillary measurement on the ^{78}Se isotope in order to discriminate ^{78}Se resonances, as shown in Figure 8. Data are in a preliminary phase of analysis.

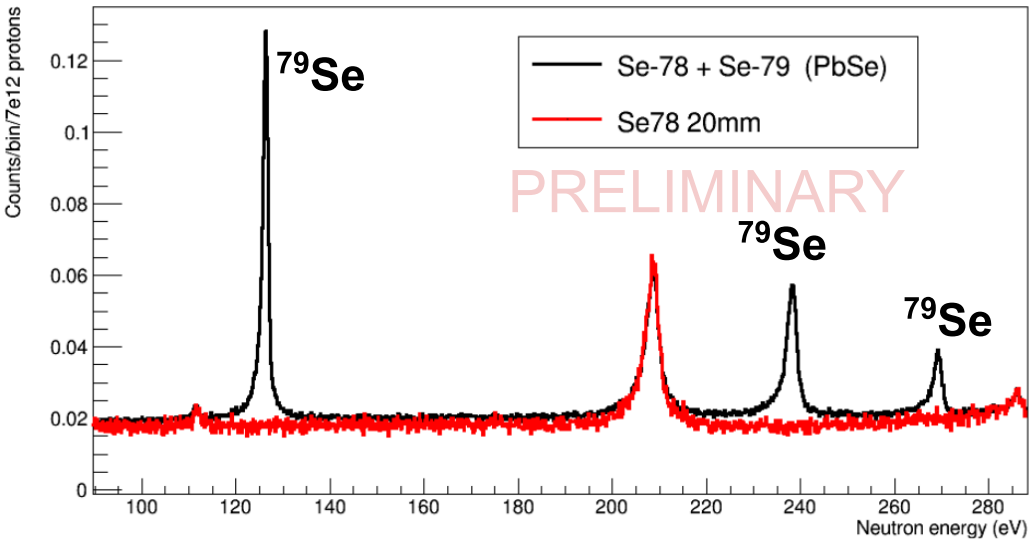

Figure 8. Comparison of measured counts from ^{79}Se(n,γ)^{80}Se and ^{78}Se(n,γ)^{79}Se reactions.

6.3. $^{94}Nb(n, \gamma)$

The neutron capture cross section of the radioactive ^{94}Nb isotope ($t_{1/2} = 2.04 \times 10^4$ years) plays a decisive role in determining the s-process production of ^{94}Mo in AGB stars, which currently cannot be reproduced by stellar models [105]. Moreover, moving through the Zr–Nb–Mo region, the neutron capture cross section of Nb addresses the different components of the nucleosynthesis s-processes (weak and main) that take place at different stars: weak component in massive stars (with mass in excess of 8–10 $M_\odot$) and main component in lower-mass stars.

Before the measurement performed at n_TOF, only two resonances were previously measured using the neutron transmission method. The measurement performed at n_TOF EAR2 could only rely on about 2×10^{19} atoms of ^{94}Nb (about 3 mg), based on hyper-pure ^{93}Nb material activated at the ILL high-flux reactor.

Thanks to a state-of-the-art detection system (based on the sTED array [92]) and the performance of the high flux beamline at EAR2 [106,107], resonances for $E_n \lesssim 1$ keV could be measured. Preliminary data of ongoing analysis indicate the observation of about 10 resonances in this energy range. Detailed analysis of them should provide enough information for the evaluation of MACS at relevant kT.

6.4. $^{151}Sm(n, \gamma)$

The ^{151}Sm(n, γ) study was the very first measurement performed at the n_TOF EAR1 [58,59]. ^{151}Sm with $t_{1/2} \approx 90$ years is one of the main branch point isotopes along the main s-process component. The competition between neutron capture and β-decay leads to a split of the reaction path at ^{151}Sm, followed by a second branching at ^{154}Eu. The additional nearby branching points ^{152,155}Eu and ^{153}Gd are of minor importance, and the branchings at ^{151}Sm and ^{154}Eu determine the abundances of the s-only isotopes ^{152}Gd and ^{154}Gd, respectively. Since the β-decay rate of ^{151}Sm depends on temperature, this branching can be used to constrain thermodynamic conditions (temperature and neutron density profiles) during the main s-process in AGB stars from the local abundance pattern in this mass range.

The measurement was performed using a sample of 156 GBq activity (206 mg), with $\simeq$90% enriched. The value extracted of the MACS at kT = 30 keV is 3.08 $\pm$ 0.15 b, and stellar models of low mass AGB stars using this MACS resulted in a consistent description of abundances in the Sm–Eu–Gd region, indicating that assumed neutron density and temperature profiles are consistent with isotopic abundance observations.

6.5. $^{171}Tm(n, \gamma)$

The unstable ^{171}Tm ($t_{1/2}$ of only 1.92 yr) is a part of a few branching points in the A $\sim$ 170 mass region, and its neutron capture cross section as a function of the neutron energy was never measured before the experiment performed at n_TOF EAR2. A wide collaboration between laboratories was required for the production for the first time of more than 3 mg of ^{171}Tm at the ILL high-flux reactor, for the preparation of a sample at the Paul Scherrer Institute (PSI) in Villigen (Switzerland), where a high enrichment of 98% was achieved, and for the final measurement at CERN.

The ^{171}Tm(n, γ) reaction is of particular interest because it affects the isotopic ratios of the Ytterbium isotopes. ^{170}Yb is an s-only isotope, shielded by stable ^{170}Er from the contribution of the r-process. The abundance of ^{170}Yb was measured in presolar SiC grains and can be used as a test of stellar models, once the ^{171}Tm(n, γ) cross section is experimentally obtained. A total of 28 resonances were observed up to 1 keV of incident neutron energy, and a MACS value at 30 keV of 570 $\pm$ 220 mb has been deduced, 17% higher than that of the Bao et al. compilation [94], used in previous astrophysical calculations.

The new result was successfully used to solve isotopic anomalies in rare-earth elements found in SiC grains of the Murchison meteorite [108]. In particular, the ^{171}Yb/^{172}Yb and ^{173}Yb/^{172}Yb isotopic ratios could be well reproduced after the new cross section measured at n_TOF with the support of detailed modeling of the so-called third dredge-ups (TDUs) included in updated stellar models of low-mass stars [109]. In fact, SiC grains are thought to be synthesized after TDUs, when by-products of nuclear burning occurring in stellar interior are mixed to the surface layer.

6.6. ^{204}Tl(n, γ)

Between-lead isotopes ^{204}Pb is the only one of pure s-process origin, because it is shielded from the r-process by its isobar ^{204}Hg. Therefore, this isotope plays a pivotal role in studying the s-process nucleosynthesis in AGB stars. This is because these nuclei can be used to benchmark state-of-the-art AGB models by comparing nucleosynthesis calculations with their observed abundances. Its abundance is strongly depending on properties of a ^{204}Tl branching point, whose $t_{1/2}$ of 3.78 years is comparable to the time scale of the neutron capture s-process. A challenging measurement was performed at EAR1. The ^{204}Tl sample for the experiment was produced from neutron irradiation of a seed sample of ^{203}Tl at the ILL high-flux reactor. The obtained ^{204}Tl concentration in the sample was 4%, corresponding to a ^{204}Tl total mass of only 9 mg (with a strong activity of 150 GBq). Thanks to the long flight path and the consequently high energy resolution of the EAR1 neutron beam, it was possible to resolve 11 ^{204}Tl capture resonances, all at $E_n < 4$ keV, from those much more prominent ones of ^{203}Tl.

The extracted MACS at the s-process temperatures of kT $\approx$ 8 keV and kT $\approx$ 30 keV [69], are about 3% lower and 20% higher, respectively, than the corresponding theoretical values widely used in nucleosynthesis simulations [100]. The ^{204}Pb abundances obtained from stellar models using the n_TOF cross sections are in agreement with the ^{204}Pb abundance measured in the solar system.

7. Neutron Sources and Poisons in the Stars

In AGB stars, the site of the main s-process, the current models consider mainly two neutron sources: the ^{13}C(α, n) reaction, responsible for producing the bulk of heavy elements, and the ^{22}Ne(α, n) reaction, only partially activated and responsible for the activation of several branching points along the s-process path. In addition, neutron poisons also produce interesting nucleosynthesis effects, whose evidence is testified by stellar observations and the abundance of isotope distributions in SiC grains.

Some of the measurements performed at n_TOF were also dedicated to produce nuclear data to accurately describe cross sections of both the neutron sources or poisons that contribute to the neutron balance in the stellar environments.

7.1. ^{14}N(n, p)

The ^{14}N(n, p)^{14}C reaction plays a key role in nuclear astrophysics because it is a significant neutron poison in the s-process nucleosynthesis. Moreover in the CNO cycle, the protons produced in this reaction present an additional poisoning effect weakening the neutron source because they remove ^{13}C nuclei through the ^{13}C(p, γ) reaction.

The measurement at EAR1 has allowed the determination of the ^{14}N(n, p) cross section over a wide energy range, from subthermal neutron energy up to 800 keV for the first time and with high accuracy of about 2.5% [76]. The first two resonances (at 492.7 and 644 keV) were resolved, and the thermal cross section (1.809 $\pm$ 0.045 b) was extracted, lower than the two most recent measurements [110,111] by more than one standard deviation, but consistent with the evaluations.

7.2. $^{25}Mg(n, \gamma)$

The ^{22}Ne(α, γ)^{26}Mg and ^{22}Ne(α, n)^{25}Mg nuclear reactions regulate the production of neutrons in both massive and in AGB stars. In particular, the ^{22}Ne(α, n)^{25}Mg neutron source is activated in AGB stars during a series of convective He-shell burning episodes, so-called thermal pulses, with temperatures as high as 400 MK. Although the contribution of the reaction to the total neutron budget is only of 5%, the effect on final abundance pattern is crucial: it is decisive for deriving information on neutron density and temperature in the He-burning layers of AGB stars. A different situation is present in massive stars, where thermal energies of ≈25 and 90 keV are reached during the He-core and C-shell burning phases, and the neutron budget is by far dominated by the ^{22}Ne(α, n)^{25}Mg reaction.

The direct measurement of the ^{22}Ne(α, n)^{25}Mg reaction is difficult due to the low cross section at low energies of α particles; the neutron emission starts at $E_\alpha = 570$ keV [112]. To address this limitation, indirect methods have been suggested, including the study of the ^{25}Mg(n, γ)^{26}Mg neutron capture [24].

Measurements of this reaction performed at EAR1 of n_TOF were carried out with highly enriched, metallic samples (97.87%), and parameters of 5 resonances were extracted in the energy region $E_n < 300$ keV, corresponding to an incident α-particle energy for reactions on ^{22}Ne from threshold to approximately 850 keV. The obtained information on resonances was useful for calculating the upper limit of the ^{22}Ne(α, n) reaction rates, based purely on experimentally available information. A 30% decrease in the upper limit of the rate with respect to the value previous present in the literature [113] has been obtained around kT = 25 keV, a temperature at which He shell burning in low-mass AGB stars and core He burning in massive stars takes place.

8. Primordial Nucleosynthesis

Measurements performed at n_TOF were not exclusively dedicated to the improvements of nuclear data of interest of stellar nucleosynthesis, but were also useful to approach primordial nucleosynthesis. In fact, the large discrepancy between the abundance of primordial ^{7}Li predicted by the standard theory of Big Bang Nucleosynthesis (BBN) and the value deduced from the observation of metal-poor stars, the so-called Cosmological Lithium Problem (CLiP) [114], representing one of the most important unresolved problems in nuclear astrophysics, has been investigated by means of the study of the ^{7}Be(n, p) and ^{7}Be(n, α) reactions. While primordial abundances of other nuclides are remarkably well reproduced by BBN calculations, ^{7}Li production is overestimated by more than a factor of 3. Possible explanations of the CLiP problem have been proposed involving several fields as nuclear physics, astrophysics [115], astronomical observations, nonstandard cosmology, and new physics beyond the standard model of particle physics, but at present, a fully satisfactory solution is still pending.

The abundance of ^{7}Li is essentially determined by the production and destruction of ^{7}Be. Indeed, the standard BBN predicts that 95% of the primordial ^{7}Li is produced by the electron capture decay of ^{7}Be, which happened at late times after the Big Bang, when the Universe cooled down sufficiently and electrons and nuclei combined into atoms.

To investigate a possible nuclear physics solution to the CLiP, several measurements have been proposed, on the basic idea that a higher rate for neutron- or charged-particle-induced reactions on ^{7}Be leads to a lower surviving ^{7}Be fraction and consequently to a lower ^{7}Li abundance.

The measurements are particularly challenging because of the high specific activity of ^{7}Be (13 GBq/μg) and low cross sections. Moreover, in the study of the (n, p) reaction, the small Q value of the reaction (1.64 MeV) leads to the emission of low-energy protons, putting severe constraints on the total mass, areal density, and purity of the samples.

The high beam luminosity in EAR2 then played a fundamental role in making these measurements possible.

The ^{7}Be sample materials were produced at PSI, by a radiochemical separation of ^{7}Be from the SINQ cooling water; separated material was then implanted on an Al backing at CERN-ISOLDE and immediately afterwards irradiated at n_TOF [116]. Implanted target contained only hundreds of ng of ^{7}Be, with a very high purity of 99%.

Two different experimental setups were adopted, both based on silicon detectors. As shown in Figure 9, a telescope made of two silicon strip detectors of 20 μm and 300 μm thicknesses for ΔE and E detection, respectively, was set/used for (n, p) reaction. The (n, α) measurement was then based on the detection of both α's emitted from the decay of ^{8}Be. In this case, a sort of sandwich made of two silicon detectors including the ^{7}Be sample was placed directly in the neutron beam.

The obtained cross sections were higher than the ones traditionally used in the BBN calculations [1], but not sufficiently high to reconcile the standard BBN Lithium yield with astrophysical observations. The deduced reaction rate leads to a minor change of the ^{7}Li yield, thus leaving the solution of the CLiP to other explanations.

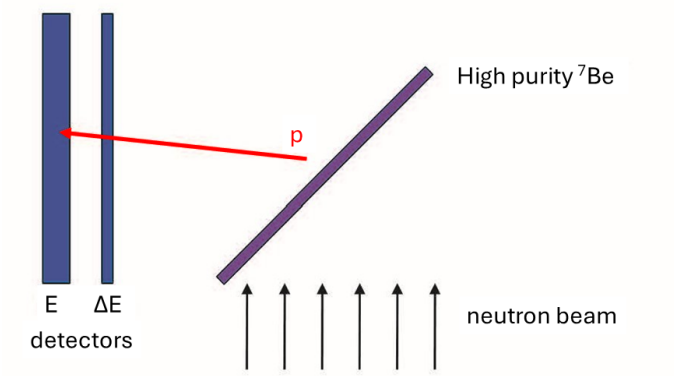

Figure 9. Sketch of the experimental setup used for the study of the ^{7}Be(n, p) reaction.

9. Cosmochronology

The time duration of the nucleosynthesis of the heavy elements produced by neutron capture processes can be used to set limits on the age of the Universe [117]. Among several cosmic clocks based on the abundances of long-lived radioactive isotopes, the ^{187}Os/^{187}Re is one of the more interesting.

The clock is based on the extremely long half-life of ^{187}Re ($t_{1/2}$ = 43.3 Gyr) against decay to ^{187}Os and on the fact that ^{186}Os and ^{187}Os are shielded against direct r-process production. Then, thanks to the well-established s-process abundances of ^{186}Os and ^{187}Os, the Re/Os clock exploits the enhancement in the abundance of ^{187}Os due to ^{187}Re β-decay.

Resonance parameters and the capture cross section have been extracted from a measurement in EAR1 in the entire range of astrophysical interest with typical uncertainties of 5%. In practice, limits in the application of the Re/Os clock come from the dramatic temperature dependence of the ^{187}Re half-life, from the necessary corrections to take into account the thermal population of excited nuclear states of the ^{187}Os isotope, and from the reliability of the model used for galactic chemical evolution. The uncertainty on the capture cross-section ratio of ^{186}Os and ^{187}Os propagates into the uncertainty of a determined age of the Universe. Thanks to the measured data, the nuclear physics uncertainties affecting the age obtained by the Re/Os clock were reduced to less than 1 Gyr, with a final result including astronomical uncertainties of 15 $\pm$ 2 Gyr [65,66], in good agreement with values obtained with different methods.

10. Cosmic γ-Ray Emitter ^{26}Al

The cosmic γ-ray emitter ^{26}Al ($t_{1/2} = 0.7$ Myr) is of high interest in astrophysics. Its presence in our galaxy provides evidence for ongoing nucleosynthesis, and the excess of its daughter isotope ^{26}Mg observed in meteoric calcium–aluminum-rich inclusions (CAIs) indicates that ^{26}Al was injected in the early solar system (see e.g., [118]). ^{26}Al abundances produced in massive stars (the main source of galactic ^{26}Al) and AGB stars sensitively depend on ^{26}Al(n, p) and ^{26}Al(n, α) reaction rates, in particular reactions on the ground state of ^{26}Al (^{26}Al has also a low-lying isomer ($E_x = 228$ keV, $T_{1/2} = 6.4$ s), which predominantly decays via β-decay, and which is not in equilibrium with the ground state below $T \approx 0.5$–1 GK [119,120]. Hence, nucleosynthesis calculations treat the ground and isomeric states as two different species at lower stellar temperatures.) [119,121]. A recent measurement of these reactions at n_TOF resulted in high accuracy reaction rates for both channels up to stellar temperatures of about 0.5 GK [77,80]. The measurement was performed at EAR2 using a unique ^{26}Al sample of $\approx 2.6 \times 10^{17}$ atoms [122]. The purpose-built silicon strip detection system consisted of a 20 µm thick single-sided silicon strip detector (SSD) as ΔE and a 50 µm thick (SSD) as E detector. The setup was optimized to minimize the detector response to the γ-flash, a prompt signal induced when the proton beam hits the spallation target, which limits the highest neutron energies which can be accessed. Neutron cross sections up to 150 keV could be obtained from this measurement, constraining stellar reaction rates in AGB stars. The n_TOF data were used in AGB stellar models and predicted isotopic Al ratios agree well with observations in meteoritic inclusions originating from AGB stars [121]. To constrain ^{26}Al production in massive stars, neutron data at higher energies are required. A new measurement of these reactions was performed in 2023 with a further optimized setup, with the aim of measuring cross sections up to $E_n \approx 500$ keV. The data are currently being analyzed.

11. Future and Perspectives

The neutron time-of-flight facility n_TOF at CERN will approach the 25th anniversary in 2026. In addition to a dense experimental program, R&D activities performed there opened the possibility to expand the fields of investigations to new, challenging measurements.

In general, MACS for studying the slow neutron capture processes requires uncertainties of about 5% to match the precision of observations and requirements of stellar models; for the present situation, see Figure 10. Since its inception, the n_TOF facility has delivered these target accuracies for many cases. However, there are a number of reactions for which better accuracies are required, or which have not been studied experimentally yet. In the following, a list of recently made or planned impactful improvements to the facility and to the experimental instrumentation is described:

1. **Measurements of highly radioactive samples or samples available in low amount of mass**
   As mentioned earlier, the high instantaneous neutron flux and excellent neutron energy resolution make the n_TOF facility well suited for measuring radioactive isotopes to suppress backgrounds from radioactivity and sample impurities. In the past years, a collaboration with several laboratories (CERN-Isolde, ILL, Joint Research Center (JRC) Geel, Los Alamos National Laboratory (LANL), PSI) that are able to isolate desired isotopes has been fruitfully established. In general, isotopes with half-lives higher than about a hundred of days available in a sufficient amount can be measured using the time-of-flight technique, while the activation technique can be applied even in more challenging physics cases.

One example is the first time-of-flight measurement of the ^{88}Zr(n, γ) reaction in 2024, during which a small amount of ^{88}Zr, 1.68 µg, $t_{1/2}$ = 83 days, was placed in EAR2 [123]. This measurement was possible thanks to an efficient collaboration between LANL for the production of the sample material, PSI for handling and preparation of the sample, and CERN for the time-of-flight measurement. Given this success, new isotopes have been added to the list of possible measurements, opening a path to measure nuclei involved in the i-process nucleosynthesis.

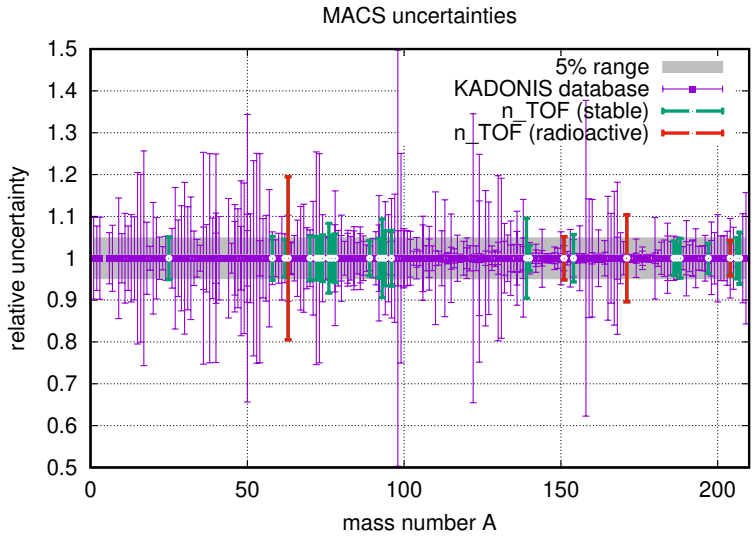

Figure 10. Uncertainties in the MACS for kT = 30 keV available in the Kadonis database [100]. The 5% band shows what is typically requested by astrophysics modeling of the s-process nucleosynthesis. MACS of stable and radioactive isotopes for which the results from n_TOF measurements have already been published is shown.

2. **Possibility to measure gaseous samples**
   Thanks to an in-house developed gas cell that can resist the pressure of hundreds of bar, a gas target, namely, ^{40}Ar, was used for the first time in 2024 at n_TOF. Given that nucleosynthesis processes involving noble gases (Ne, Ar and Kr) take place for kT from few to hundreds keV, depending on the stellar conditions [124], new neutron capture measurements can be scheduled in the near future.
   An opportunity to work with liquid target will be definitely exploited too.
3. **Installation of a neutron transmission station**
   A full description of parameters of individual resonances, i.e., energy, neutron and γ widths, spin and parity, can be often extracted from the combined analysis of capture and transmission measurements. In transmission experiments, the observed quantity is the fraction of the neutron beam that passes through the sample without any interaction. The transmission factor is obtained from the ratio of a sample-in and a sample-out measurement, both corrected for dead-time effects and background contributions.
   Recent tests and engineering studies have been conducted to set up a transmission station in the neutron beamline leading to EAR1. The first measurement on ^{63,65}Cu isotopes was performed in 2025.
4. **Use of activation measurements**
   Another chance to overcome the limits of measurements on isotopes available with a very low mass and/or with a short decay time can be to exploit the activation technique, using the high neutron fluxes available at the NEAR station. The activation technique consists of irradiation of the sample of interest and subsequent radioactive decay counting. Hence, this technique is limited to cases where the reaction product is unstable.

At the NEAR station, about 3 m from the neutron spallation target, the method of filtering the neutron spectrum has been developed. This method allows for using absorbers in the neutron beam to create quasi-stellar neutron spectra and hence directly measure an averaged cross section. Use of these "quasi-stellar" spectra corresponding to different T for measurements of MACS is planned. Such measurements will be particularly beneficial for unstable or low-mass samples, for cases in which extremely low reaction rates are expected. Furthermore, future plans include implementing the fast cyclic activation technique, allowing for performing activation measurements on short-lived reaction products, particularly important for new astrophysical scenarios such those envisaged by the i-process.

In addition, the collaboration was recently proposed to install a neutron activation station n_ACT at the recently endorsed SPS Beam Dump Facility (BDF), which will operate the Search for Hidden Particles (SHiP) experiment [125]. At the core of this facility, a high-Z spallation target/dump will be located to absorb proton beams at 400 GeV/c with an intensity of 4×10^{13} protons per proton pulse, with an average beam power of roughly 350 kW, most of it fully deposited in the target. The expected neutron flux at n_ACT will be about a factor 1000 higher than at the NEAR activation station. An expression of interest has been submitted to the CERN SPS and PS Experiments Committee, and a full proposal is currently under preparation.

12. Summary

The n_TOF facility at CERN is going to celebrate a quarter of a century of its operation. The research activities on neutron-induced reactions has delivered during these 25 years key data for astrophysics in understanding the origin of the chemical elements in the Universe, in particular for the slow neutron capture nucleosynthesis (s-process). Nuclear data with unprecedented accuracy (e.g., MACS extracted with uncertainties lower than 5%) in broad energy domains are routinely produced at the n_TOF facility. Several tens of experimental investigations relevant for astrophysics have been performed so far (see Tables 1 and 2), and data sets have been uploaded in the Experimental Nuclear Reaction Database (EXFOR, maintained by IAEA). More than 150 researchers representing more than 40 research teams or institutes, primarily located within Europe, including an average of 20 PhD students, give life to a dynamic international collaboration, ensuring a broad list of proposals and studies on new physics cases.

Recently made and planned upgrades will further enhance the capabilities of the facility, enabling a wider area of research. These improvements include a new transmission station, a moderator for the NEAR station, high-pressure gas cells for gaseous targets, and R&D of advanced detectors to widen the range of nuclear reaction channels that can be exploited. A bright future promising even more accurate results from n_TOF is envisaged.

Author Contributions: First draft worked by P.M.M., the paper was finalized with improvements suggested by C.L.-W. and A.M. All authors have read and agreed to the published version of the manuscript.

Funding: Support of funding agencies of all institutions participating at n_TOF is acknowledged.

Data Availability Statement: Data are contained within the article.

Conflicts of Interest: The authors declare no conflict of interest.

Abbreviations

The following abbreviations are used in this manuscript:

AGB	Asymptotic Giant Branch
CERN	European Council for Nuclear Research
CLiP	Cosmological Lithium Problem
IAEA	International Atomic Energy Agency
ILL	Institute Laue–Langevin
JRC	Joint Research Center
LANL	Los Alamos National Laboratory
MACS	Maxwellian Averaged Cross Section
n_TOF	neutron Time Of Flight
PSI	Paul Scherrer Institute
SEF	Stellar Enhanced factor
sTED	segmented Total Energy Detector
TAC	Total Absorption Calorimeter

Appendix A. Membership of The n_TOF Collaboration

P. M. Milazzo [1,2,*], C. Lederer-Woods [3], A. Mengoni [2,4], O. Aberle [2], V. Alcayne [5], G. Alpar [6], S. Amaducci [7], V. Babiano [8], M. Bacak [2,9,10], J. Balibrea-Correa [11], J. Bartolomé [12], A. P. Bernardes [2], B. Bernardino Gameiro [11], E. Berthoumieux [13], R. Beyer [14], M. Birch [9], M. Boromiza [15], M. Caamaño [16], A. Cahuzac [13], F. Calviño [8], M. Calviani [2], D. Cano-Ott [5], A. Casanovas [8], D. M. Castelluccio [4,17], F. Cerutti [2], G. Cescutti [1,18], E. Chiaveri [2,9], G. Claps [19], P. Colombetti [20,21], N. Colonna [22], P. Console Camprini [4,17], G. Cortés [8], M. A. Cortés-Giraldo [12], L. Cosentino [7], S. Cristallo [23,24], G. de la Fuente Rosales [11], S. F. Dellmann [25], M. Diakaki [26], A. Di Chicco [27], M. Dietz [27], C. Domingo-Pardo [11], E. Dupont [13], I. Durán [16], Z. Eleme [28], M. Eslami [29], B. Fernández-Domínguez [16], P. Finocchiaro [7], W. Flanagan [6], V. Furman [30], A. Gandhi [15], F. García-Infantes [2,3,31], A. Gawlik-Ramięga [32], G. Gervino [20,21], S. Gilardoni [2], E. González-Romero [5], S. Goula [28], E. Griesmayer [10], C. Guerrero [12], F. Gunsing [13], C. Gustavino [33], J. Heyse [34], D. G. Jenkins [29], E. Jericha [10], A. Junghans [14], Y. Kadi [2], K. Kaperoni [26], I. Kelly [6], M. Kokkoris [26], Y. Kopatch [30], M. Krtička [35], N. Kyritsis [26], J. Lerendegui-Marco [11], A. Manna [2,17], M. Martínez-Cañada [31], A. Masi [2], C. Massimi [17,36], P. Mastinu [37], M. Mastromarco [22], E. A. Maugeri [38], A. Mazzone [22,39], E. Mendoza [5], V. Michalopoulou [26], J. Moldenhauer [6], R. Mucciola [22], E. Musacchio González [37], A. Musumarra [40,41], A. Negret [15], E. Odusina [3], D. Papanikolaou [40], N. Patronis [28], J. A. Pavón-Rodríguez [12], M. G. Pellegriti [40], P. Pérez-Maroto [8], G. Perfetto [22], J. Perkowski [32], C. Petrone [15], N. Pieretti [17,36], L. Piersanti [23,24], E. Pirovano [27], I. Porras [31], J. Praena [31], J. M. Quesada [12], R. Reifarth [25], A. Reina-Conde [12], D. Rochman [38], Y. Romanets [42], A. Rooney [3], G. Rovira [43], C. Rubbia [2], A. Sánchez-Caballero [5], R. N. Sahoo [17], P. Schillebeeckx [34], A. G. Smith [9], N. V. Sosnin [3,9], M. Spelta [1,18], M. E. Stamati [2,26], K. Stasiak [32], G. Tagliente [22], A. Tarifeño-Saldivia [11], D. Tarrío [44], P. Torres-Sánchez [11], S. Tosi [19], G. Tsiledakis [13], S. Valenta [35], P. Vaz [42], D. Vescovi [23,24], V. Vlachoudis [2], R. Vlastou [26], A. Wallner [14], C. Weiss [10], P. J. Woods [3], T. Wright [9] and R. Wu [29]

Affiliations

1 Istituto Nazionale di Fisica Nucleare, Sezione di Trieste, 34149 Trieste, Italy
2 European Organization for Nuclear Research (CERN), 1211 Geneva, Switzerland
3 School of Physics and Astronomy, University of Edinburgh, Edinburgh EH9 3FD, UK
4 Agenzia Nazionale per le Nuove Tecnologie (ENEA), 40129 Bologna, Italy
5 Centro de Investigaciones Energéticas Medioambientales y Tecnológicas (CIEMAT), 28040 Madrid, Spain

[6] University of Dallas, 1845 East Northgate Drive, Irving, Texas 75062-4736, USA
[7] Istituto Nazionale di Fisica Nucleare, Laboratori Nazionali del Sud, 95125 Catania, Italy
[8] Universitat Politècnica de Catalunya, 08034 Barcelona, Spain
[9] University of Manchester, Manchester M13 9PL, UK
[10] Technische Universität Wien, 1040 Vienna, Austria
[11] Instituto de Física Corpuscular, CSIC—Universidad de Valencia, 46980 Paterna, Spain
[12] Universidad de Sevilla, 41004 Sevilla, Spain
[13] CEA Irfu, Université Paris-Saclay, F-91191 Gif-sur-Yvette, France
[14] Helmholtz-Zentrum Dresden-Rossendorf, 01328 Dresden, Germany
[15] Horia Hulubei National Institute of Physics and Nuclear Engineering, P.O. Box MG-6, RO-76900 Bucharest, Romania
[16] University of Santiago de Compostela, Santiago de Compostela, 15705 Compostela, Spain
[17] Istituto Nazionale di Fisica Nucleare, Sezione di Bologna, 40127 Bologna, Italy
[18] Department of Physics, University of Trieste, 34149 Trieste, Italy
[19] Istituto Nazionale di Fisica Nucleare, Laboratori Nazionali di Frascati, 00044 Frascati (Roma), Italy
[20] Istituto Nazionale di Fisica Nucleare, Sezione di Torino, 10125 Torino, Italy
[21] Department of Physics, University of Torino, 10125 Torino, Italy
[22] Istituto Nazionale di Fisica Nucleare, Sezione di Bari, 70121 Bari, Italy
[23] Istituto Nazionale di Fisica Nucleare, Sezione di Perugia, 06123 Perugia, Italy
[24] Istituto Nazionale di Astrofisica—Osservatorio Astronomico d'Abruzzo, 64100 Collurania, Italy
[25] Goethe University Frankfurt, 60323 Frankfurt am Main, Germany
[26] National Technical University of Athens, Athens, 10682, Greece
[27] Physikalisch-Technische Bundesanstalt (PTB), Bundesallee 100, 38116 Braunschweig, Germany
[28] University of Ioannina, 451 10 Ioannina, Greece
[29] University of York, York YO10 5DD, UK
[30] Affiliated with an Institute Covered by a Cooperation Agreement with CERN
[31] University of Granada, 18010 Granada, Spain
[32] University of Lodz, 90-137 Łódź, Poland
[33] Istituto Nazionale di Fisica Nucleare, Sezione di Roma1, 00185 Roma, Italy
[34] European Commission, Joint Research Centre, Geel, Retieseweg 111, B-2440 Geel, Belgium
[35] Charles University, 11000 Prague, Czech Republic
[36] Dipartimento di Fisica e Astronomia, Universitá di Bologna, 40129 Bologna, Italy
[37] Istituto Nazionale di Fisica Nucleare, Laboratori nazionali di Legnaro, 35020 Legnaro (Padova), Italy
[38] Paul Scherrer Institut (PSI), 5232 Villigen, Switzerland
[39] Consiglio Nazionale delle Ricerche, 00185 Bari, Italy
[40] Istituto Nazionale di Fisica Nucleare, Sezione di Catania, 95123 Catania, Italy
[41] Department of Physics and Astronomy, University of Catania, 95131 Catania, Italy
[42] Instituto Superior Técnico, 1049-001 Lisbon, Portugal
[43] Japan Atomic Energy Agency (JAEA), Tokai-mura 319-1184, Japan
[44] Department of Physics and Astronomy, Uppsala University, 75120 Uppsala, Sweden
* Correspondence: paolo.milazzo@ts.infn.it

References

1. Wagoner, R.V.; Fowler, W.A.; Hoyle, F. Synthesis of Elements at very high Temperatures. *Astrophys. J.* **1967**, *148*, 3. [CrossRef]
2. Schramm, D.N.; Turner, M.S. Big-bang nucleosynthesis enters the precision era. *Rev. Mod. Phys.* **1998**, *70*, 303. [CrossRef]
3. Pitrou, C.; Coc, A.; Uzan, J.P.; Vangioni, E. Precision big bang nucleosynthesis with improved Helium-4 predictions. *Phys. Rep.* **2018**, *754*, 1. [CrossRef]
4. Alpher, R.A.; Bethe, H.A.; Gamow, G. The Origin of Chemical Elements. *Phys. Rev.* **1948**, *73*, 803. [CrossRef]
5. Burbidge, E.M.; Burbidge, G.R.; Fowler, W.A.; Hoyle, F. Synthesis of the Elements in Stars. *Rev. Mod. Phys.* **1957**, *29*, 547. [CrossRef]
6. Cameron, A.G.W. *Stellar Evolution, Nuclear Astrophysics, and Nucleogenesis*, 2nd ed.; Technical Report; Courier Corporation: North Chelmsford, MA, USA, 1957.
7. Suess, H.E.; Urey, H.C. Abundances of the Elements. *Rev. Mod. Phys.* **1956**, *28*, 53. [CrossRef]
8. Cameron, A.G.W. Abundances of the elements in the solar system. *Space Sci. Rev.* **1973**, *15*, 121. [CrossRef]
9. Anders, E.; Grevesse, N. Abundances of the elements: Meteoritic and solar. *Geochim. Cosmochim. Acta* **1989**, *53*, 197. [CrossRef]
10. Asplund, M.; Grevesse, N.; Jacques Sauval, A.; Scott, P. The Chemical Composition of the Sun. *Annu. Rev. Astron. Astrophys.* **2009**, *47*, 481. [CrossRef]
11. Käppeler, F.; Gallino, R.; Bisterzo, S.; Aoki, W. The s-process: Nuclear physics, stellar models, and observations. *Rev. Mod. Phys.* **2011**, *83*, 157. [CrossRef]
12. Lodders, K. Relative Atomic Solar System Abundances, Mass Fractions, and Atomic Masses of the Elements and Their Isotopes, Composition of the Solar Photosphere, and Compositions of the Major Chondritic Meteorite Groups. *Space Sci. Rev.* **2021**, *217*, 44. [CrossRef]
13. Cowan, J.J.; Sneden, C.; Lawler, J.E.; Aprahamian, A.; Wiescher, M.; Langanke, K.; Martínez-Pinedo, G.; Thielemann, F.K. Origin of the heaviest elements: The rapid neutron-capture process. *Rev. Mod. Phys.* **2021**, *93*, 015002. [CrossRef]
14. Arlandini, C.; Käppeler, F.; Wisshak, K.; Gallino, R.; Lugaro, M. Neutron capture in low mass asymptotic giant branch stars: cross-sections and abundance signatures. *Astrophys. J.* **1999**, *525*, 886. [CrossRef]
15. Sneden, C.; Cowan, J.J.; Gallino, R. Neutron-capture elements in the early galaxy. *ARA&A* **2008**, *46*, 241.
16. Prantzos, N.; Abia, C.; Cristallo, S.; Limongi, M.; Chieffi, A. Chemical evolution with rotating massive star yields II. A new assessment of the solar s- and r-process components. *Mon. Not. R. Astron. Soc.* **2020**, *491*, 1832. [CrossRef]
17. Straniero, O.; Gallino, R.; Cristallo, S. s-process in low-mass asymptotic giant branch stars. *Nucl. Phys. A* **2006**, *777*, 311. [CrossRef]
18. Karakas, A.I.; Lattanzio, J.C. The dawes review 2: Nucleosynthesis and stellar yields of low- and intermediate-mass single stars. *Pub. Astron. Soc. Aust.* **2014**, *31*, e030. [CrossRef]
19. Peters, J.G. Nucleosynthesis by the s-process in stars of 9 and 15 Solar Masses. *Astrophys. J.* **1968**, *154*, 225. [CrossRef]
20. Heil, M.; Käppeler, F.; Uberseder, E.; Gallino, R.; Pignatari, M. The s process in massive stars. *Prog. Part. Nucl. Phys.* **2007**, *59*, 174. [CrossRef]
21. Choplin, A.; Siess, L.; Goriely, S. The intermediate neutron capture process. *Astron. Astrophys.* **2021**, *648*, A119. [CrossRef]
22. Vescovi, D.; Cristallo, S.; Busso, M.; Liu, N. Magnetic-buoyancy-induced Mixing in AGB Stars: Presolar SiC Grains. *Astrophys. J. Lett.* **2020**, *897*, L25. [CrossRef]
23. Massimi, C.; Koehler, P.; Bisterzo, S.; Colonna, N.; Gallino, R.; Gunsing, F.; Käppeler, F.; Lorusso, G.; Mengoni, A.; Pignatari, M.; et al. Resonance neutron-capture cross sections of stable magnesium isotopes and their astrophysical implications. *Phys. Rev. C* **2012**, *85*, 044615. [CrossRef]
24. Massimi, C.; Altstadt, S.; Andrzejewski, J.; Audouin, L.; Barbagallo, M.; Bécares, V.; Belloni, F.; Berthoumieux, E.; Billowes, J.; Bisterzo, S.; et al. Neutron spectroscopy of ^{26}Mg states: Constraining the stellar neutron source ^{22}Ne(α, n)^{25}Mg. *Phys. Lett. B* **2017**, *768*, 1. [CrossRef]
25. Lederer-Woods, C.; Mengoni, A.; Andrzejewski, J.; Boromiza, M.; Casanovas, A.; Cristallo, S.; Dietz, M.; Domingo-Pardo, C.; Gawlik-Ramiega, A.; Gervino, G.; et al. CERN-INTC-2023-009; Measurement of ^{28,29,30}Si(n, γ) Capture Cross Sections to Explain Isotopic Abundances in Presolar Grains, INTC-P-653. Available online: http://cds.cern.ch/record/2845928 (accessed on 19 September 2025).
26. Andringa, S.; Bacak, M.; Bezawada, Y.; Boissevain, J.; Cano-Ott, D.; Carrara, N.; Casanovas, A.; Gollapinni, S.; Huang, J.; Johnson, W.; et al. Multiple Argon Experiments at n_TOF (the MArEX Initiative), CERN-INTC-2023-046; INTC-I-256. Available online: https://cds.cern.ch/record/2856506 (accessed on 19 September 2025).
27. Giubrone, G.; Domingo-Pardo, C.; Tain, J.L.; Lederer, C.; Altstadt, S.; Andrzejewski, J.; Audouin, L.; Barbagallo, M.; Bécares, V.; Bečvář, F.; et al. Measurement of the ^{54,57}Fe(n, γ) Cross Section in the Resolved Resonance Region at CERN n_TOF. *Nucl. Data Sheets* **2014**, *119*, 117. [CrossRef]
28. Žugec, P.; Barbagallo, M.; Colonna, N.; Bosnar, D.; Altstadt, S.; Andrzejewski, J.; Audouin, L.; Bécares, V.; Bečvář, F.; Belloni, F.; et al. Experimental neutron capture data of ^{58}Ni from the CERN n_TOF facility. *Phys. Rev. C* **2014**, *89*, 014605. [CrossRef]

29. Lederer, C.; Massimi, C.; Berthoumieux, E.; Colonna, N.; Dressler, R.; Guerrero, C.; Gunsing, F.; Käppeler, F.; Kivel, N.; Pignatari, M.; et al. ^{62}Ni(n, γ) and ^{63}Ni(n, γ) cross sections measured at the n_TOF facility at CERN. *Phys. Rev. C* **2014**, *89*, 025810. [CrossRef]
30. Lederer, C.; Massimi, C.; Altstadt, S.; Andrzejewski, J.; Audouin, L.; Barbagallo, M.; Bécares, V.; Bečvář, F.; Belloni, F.; Berthoumieux, E.; et al. Neutron Capture Cross Section of Unstable ^{63}Ni: Implications for Stellar Nucleosynthesis. *Phys. Rev. Lett.* **2013**, *110*, 022501. [CrossRef]
31. Tagliente, G.; Cescutti, G.; Colonna, N.; Cristallo, S.; Diacono, D.; Lederer-Wood, C.; Massimi, C.; Mastromarco, M.; Mazzone, A.M.; Milazzo, P.M.; et al. Measurement of the Neutron Capture Cross Section of ^{64}Ni, CERN-INTC-2022-033; INTC-P-208-ADD-1. Available online: http://cds.cern.ch/record/2809947 (accessed on 19 September 2025).
32. Gawlik, A.; Lederer-Woods, C.; Andrzejewski, J.; Battino, U.; Ferreira, P.; Gunsing, F.; Heinitz, S.; Krtička, M.; Massimi, C.; Mingrone, F.; et al. Measurement of the ^{70}Ge(n, γ) cross section up to 300 keV at the CERN n_TOF facility. *Phys. Rev. C* **2019**, *100*, 045804. [CrossRef]
33. Dietz, M.; Lederer-Woods, C.; Tattersall, A.; Battino, U.; Gunsing, F.; Heinitz, S.; Krtička, M.; Lerendegui-Marco, J.; Reifarth, R.; Valenta, S.; et al. Measurement of the ^{72}Ge(n, γ) cross section over a wide neutron energy range at the CERN n_TOF facility. *Phys. Rev. C* **2021**, *103*, 045809. [CrossRef]
34. Lederer-Woods, C.; Battino, U.; Ferreira, P.; Gawlik, A.; Guerrero, C.; Gunsing, F.; Heinitz, S.; Lerendegui-Marco, J.; Mengoni, A.; Reifarth, R.; et al. Measurement of ^{73}Ge(n, γ) cross sections and implications for stellar nucleosynthesis. *Phys. Lett. B* **2019**, *790*, 458. [CrossRef]
35. Lederer-Woods, C.; Aberle, O.; Andrzejewski, J.; Audouin, L.; Bécares, V.; Bacak, M.; Balibrea, J.; Barbagallo, M.; Barros, S.; Battino, U.; et al. ^{74}Ge(n, γ) cross section below 70 keV measured at n_TOF CERN. *Eur. Phys. J. A* **2022**, *58*, 239 [CrossRef]
36. Gawlik-Ramiega, A.; Lederer-Woods, C.; Krtička, M.; Valenta, S.; Battino, U.; Andrzejewski, J.; Perkowski, J.; Aberle, O.; Audouin, L.; Bacak, M.; et al. Measurement of the ^{76}Ge(n, γ) cross section at the n_TOF facility at CERN. *Phys. Rev. C* **2021**, *104*, 044610. [CrossRef]
37. Sosnin, N.V.; Lederer-Woods, C.; Krtička, M.; Garg, R.; Dietz, M.; Bacak, M.; Barbagallo, M.; Battino, U.; Cristallo, S.; Damone, L.A.; et al. Measurement of the ^{77}Se(n, γ) cross section up to 200 keV at the n_TOF facility at CERN. *Phys. Rev. C* **2023**, *107*, 065805. [CrossRef]
38. Sosnin, N.V.; Lederer-Woods, C.; Garg, R.; Battino, U.; Cristallo, S.; Dietz, M.; Heinitz, S.; Krtička, M.; Reifart, R.; Valenta, S.; et al. Measurement of the ^{78}Se(n, γ)^{79}Se cross section up to 600 keV at the n_TOF facility at CERN. *Phys. Rev. C* **2024**, *110*, 065805. [CrossRef]
39. Lerendegui-Marco, J.; Babiano-Suárez, V.; Balibrea-Correa, J.; Domingo-Pardo, C.; Ladarescu, I.; Tarifeño-Saldivia, A.; Alcayne, V.; Cano-Ott, D.; González-Romero, E.; Martínez, T.; et al. New detection systems for an enhanced sensitivity in key stellar (n, γ) measurements. *EPJ Web Conf.* **2023**, *279*, 13001. [CrossRef]
40. Babiano-Suarez, V.; Balibrea-Correa, J.; Caballero-Ontanaya, L.; Domingo-Pardo, C.; Ladarescu, I.; Lerendegui-Marco, J.; Tain, J.L.; Calviño, F.; Casanovas, A.; Tarifeño-Saldivia, A.; et al. First ^{80}Se(n, γ) cross section measurement with high resolution in the full stellar energy range 1 eV - 100 keV and its astrophysical implications for the s-process. *EPJ Web Conf.* **2022**, *260*, 11026. [CrossRef]
41. Gunsing, F.; Maugeri, E.A.; Berthoumieux, E.; Cahuzac, A.; Dupont, E.; Rochman, D.; Tsiledakis, G. Measurement of the Neutron Capture Cross Section of ^{87}Sr, CERN-INTC-2024-062; INTC-P-717. Available online: https://cds.cern.ch/record/2912215 (accessed on 19 September 2025).
42. Tagliente, G.; Milazzo, P.M.; Paradela, C.; Kopecky, S.; Vescovi, D.; Alaerts, G.; Damone, L.A.; Heyse, J.; Krtička, M.; Schillebeeckx, P.; et al. High-resolution cross section measurements for neutron interactions on ^{89}Y with incident neutron energies up to 95 keV. *Eur. Phys. J. A* **2024**, *60*, 21. [CrossRef]
43. Tagliente, G.; Fujii, K.; Milazzo, P.M.; Moreau, C.; Aerts, G.; Abbondanno, U.; Álvarez, H.; Alvarez-Velarde, F.; Andriamonje, S.; Andrzejewski, J.; et al. Neutron capture cross section of ^{90}Zr: Bottleneck in the s-process reaction flow. *Phys. Rev. C* **2008**, *77*, 035802. [CrossRef]
44. Tagliente, G.; Milazzo, P.M.; Fujii, K.; Aerts, G.; Abbondanno, U.; Álvarez, H.; Alvarez-Velarde, F.; Andriamonje, S.; Andrzejewski, J.; Assimakopoulos, P.; et al. Experimental study of the ^{91}Zr(n, γ) reaction up to 26 keV. *Phys. Rev. C* **2008**, *78*, 045804. [CrossRef]
45. Tagliente, G.; Milazzo, P.M.; Fujii, K.; Abbondanno, U.; Aerts, G.; Álvarez, H.; Alvarez-Velarde, F.; Andriamonje, s.; Andrzejewski, J.; Audouin, L.; et al. The ^{92}Zr(n, γ4) reaction and its implications for stellar nucleosynthesis. *Phys. Rev. C* **2010**, *81*, 055801. [CrossRef]
46. Tagliente, G.; Kopecky, S.; Heyse, J.; Krtička, M.; Massimi, C.; Mengoni, A.; Milazzo, P.M.; Plompen, A.j.M.; Schillebeeckx, P.; Valenta, S.; et al. ^{92}Zr(n, γ) and (n, tot) measurements at the GELINA and n_TOF facilities. *Phys. Rev. C* **2022**, *105*, 025805. [CrossRef]
47. Tagliente, G.; Milazzo, P.M.; Fujii, K.; Abbondanno, U.; Aerts, G.; Álvarez, H.; Alvarez-Velarde, F.; Andriamonje, S.; Andrzejewski, J.; Audouin, L.; et al. The ^{93}Zr(n, γ) reaction up to 8 keV neutron energy. *Phys. Rev. C* **2013**, *87*, 014622. [CrossRef]

48. Tagliente, G.; Milazzo, P.M.; Fujii, K.; Abbondanno, U.; Aerts, G.; Álvarez, H.; Alvarez-Velarde, F.; Andriamonje, S.; Andrzejewski, J.; Audouin, L.; et al. Neutron capture on ^{94}Zr: Resonance parameters and Maxwellian-averaged cross sections. *Phys. Rev. C* **2011**, *84*, 015801. [CrossRef]
49. Tagliente, G.; Milazzo, P.M.; Fujii, K.; Abbondanno, U.; Aerts, G.; Álvarez, H.; Alvarez-Velarde, F.; Andriamonje, S.; Andrzejewski, J.; Audouin, L.; et al. ^{96}Zr(n, γ) measurement at the n TOF facility at CERN. *Phys. Rev. C* **2011**, *84*, 055802. [CrossRef]
50. Babiano, V.; Balibrea-Correa, J.; Caballero, L.; Calviño, F.; Casanovas, A.; Cristallo, S.; Domingo-Pardo, C.; Dressler, R.; Guerrero, C.; Heinitz, S.; et al. First Measurement of the ^{94}Nb(n, γ) Cross-Section, CERN-INTC-2020-062; INTC-P-577. Available online: https://cds.cern.ch/record/2731959 (accessed on 19 September 2025).
51. Busso, M.; Castelluccio, D.M.; Console Camprini, P.; Colonna, N.; Cristallo, S.; Domingo-Pardo, C.; Guglielmelli, A.; Heyse, J.; Kopecky, S.; Lederer-Woods, C.; et al. Measurement of ^{92,97,98,100}Mo(n, γ) Relevant to Astrophysics and Nuclear Technology, CERN-INTC-2024-032; INTC-P-569-ADD-1. Available online: https://cds.cern.ch/record/2894937 (accessed on 19 September 2025).
52. Busso, M.; Castelluccio, D.M.; Console Camprini, P.; Colonna, N.; Cristallo, S.; Domingo-Pardo, C.; Guglielmelli, A.; Heyse, J.; Kopecky, S.; Lederer-Woods, C.; et al. Measurement of ^{94,95,96}Mo(n, γ) Relevant to Astrophysics and Nuclear Technology, CERN-INTC-2020-052; INTC-P-569. Available online: https://cds.cern.ch/record/2730968 (accessed on 19 September 2025).
53. Mucciola, R.; Tagliente, G.; Bacak, M.; Colonna, N.; Cristallo, S.; Eleme, Z.; Lugaro, M.; Manna, A.; Massimi, C.; Mastromarco, M.; et al. Measurement of ^{121,123}Sb(n, γ) Relevant to Nuclear Astrophysics, CERN-INTC-2025-033; INTC-P-744. Available online: https://cds.cern.ch/record/2929687 (accessed on 19 September 2025).
54. Terlizzi, R.; Abbondanno, U.; Aerts, G.; Álvarez, H.; Alvarez-Velarde, F.; Andriamonje, S.; Andrzejewski, J.; Assimakopoulos, P.; Audouin, L.; Badurek, G.; et al. The ^{139}La(n, γ) cross section: Key for the onset of the s-process. *Phys. Rev. C* **2007**, *75*, 033807. [CrossRef]
55. Amaducci, S.; Colonna, N.; Cosentino, L.; Cristallo, S.; Finocchiaro, P.; Krtička, M.; Massimi, C.; Mastromarco, M.; Mazzone, A.; Maugeri, E.A.; et al. Measurement of the ^{140}Ce(n, γ) Cross Section at n_TOF and Its Astrophysical Implications for the Chemical Evolution of the Universe. *Phys. Rev. Lett.* **2024**, *132*, 122701. [CrossRef]
56. Amaducci, S.; Colonna, N.; Cosentino, L.; Cristallo, S.; Finocchiaro, P.; Krtička, M.; Massimi, C.; Mastromarco, M.; Mazzone, A.; Mengoni, A.; et al. First Results of the ^{140}Ce(n, γ)^{141}Ce Cross-Section Measurement at n_TOF. *Universe* **2021**, *7*, 200. [CrossRef]
57. Lerendegui-Marco, J.; Domingo-Pardo, C.; Gameiro, B.; Babiano-Suárez, V.; Bacak, M.; Balibrea-Correa, J.; Calviño, F.; Casanovas, A.; Cortés, G.; Cristallo, S.; et al. New Measurement of the ^{146}Nd(n, γ) Cross Section at n_TOF-EAR2, CERN-INTC-2023-055; INTC-P-671. Available online: https://cds.cern.ch/record/2872360 (accessed on 19 September 2025).
58. Abbondanno, U.; Aerts, G.; Alvarez-Velarde, F.; Álvarez-Pol, H.A.; Andriamonje, S.; Andrzejewski, J.; Badurek, G.; Baumann, P.; Bečvář, F.; Benlliure, J.; et al. Neutron Capture Cross Section Measurement of ^{151}Sm at the CERN Neutron Time of Flight Facility (n_TOF). *Phys. Rev. Lett.* **2004**, *93*, 161103. [CrossRef]
59. Marrone, S.; Abbondanno, U.; Aerts, G.; Alvarez-Velarde, F.; Álvarez-Pol, H.A.; Andriamonje, S.; Andrzejewski, J.; Badurek, G.; Baumann, P.; Bečvář, F.; et al. Measurement of the ^{151}Sm(n, γ) cross section from 0.6 eV to 1 MeV via the neutron time-of-flight technique at the CERN n_TOF facility. *Phys. Rev. C* **2006**, *73*, 034604. [CrossRef]
60. Mazzone, A.; Cristallo, S.; Aberle, O.; Alaerts, G.; Alcayne, V.; Amaducci, S.; Andrzejewski, J.; Audouin, L.; Babiano-Suarez, V.; Bacak, M.; et al. Measurement of the ^{154}Gd(n, γ) cross section and its astrophysical implications. *Phys. Lett. B* **2020**, *804*, 135405. [CrossRef]
61. Mastromarco, M.; Colonna, N.; Cristallo, S.; Massimi, C.; Mengoni, A.; Tagliente, G. Measurement of the Neutron Capture Cross Section of Gadolinium-160, CERN-INTC-2021-052; INTC-P-437-ADD-1. Available online: http://cdsweb.cern.ch/record/2782347 (accessed on 19 September 2025).
62. Gawlik-Ramiega, A.; Alcayne, V.; Cano-Ott, D.; González-Romero, E.; Köster, U.; Martínez, T.; Mendoza, E.; Pérez de Rada Fiol, A.; Perkowski, J.; Sánchez-Caballero, A.; et al. Measurement of the ^{164}Er(n, γ) Cross-Section at n_TOF EAR1, CERN-INTC-2025-025; INTC-P-737. Available online: https://cds.cern.ch/record/2929553 (accessed on 19 September 2025).
63. Guerrero, C.; Lerendegui-Marco, J.; Paul, M.; Tessler, M.; Heinitz, S.; Domingo-Pardo, C.; Cristallo, S.; Dressler, R.; Halfon, S.; Kivel, N.; et al. Neutron Capture on the s-Process Branching Point ^{171}Tm via Time-of-Flight and Activation. *Phys. Rev. Lett.* **2020**, *125*, 142701. [CrossRef]
64. García-Infantes, F.; Praena, J.; Casanovas-Hoste, A.; Henkelmann, R. Kø'ster, U.; Aberle, O.; Alcayne, V.; Altieri, S.; Amaducci, S.; Amar Es-Sghir, H.; et al. Measurement of the ^{176}Yb(n, γ) cross section at the n_TOF facility at CERN. *Phys. Rev. C* **2024**, *110*, 064619. [CrossRef]
65. Mosconi, M.; Fujii, K.; Mengoni, A.; Domingo-Pardo, C.; Käppeler, F.; Abbondanno, U.; Aerts, G.; Álvarez-Pol, H.; Alvarez-Velarde, F.; Andriamonje, S.; et al. Neutron physics of the Re/Os clock. I. Measurement of the (n, γ) cross sections of ^{186,187,188}Os at the CERN n_TOF facility. *Phys. Rev. C* **2010**, *82*, 015802. [CrossRef]
66. Fujii, K.; Mosconi, M.; Mengoni, A.; Domingo-Pardo, C.; Käppeler, F.; Abbondanno, U.; Aerts, G.; Álvarez-Pol, H.; Alvarez-Velarde, F.; Andriamonje, S.; et al. Neutron physics of the Re/Os clock. III. Resonance analyses and stellar (n, γ) cross sections of ^{186,187,188}Os. *Phys. Rev. C* **2010**, *82*, 015804. [CrossRef]

67. Massimi, C.; Domingo-Pardo, C.; Vannini, G.; Audouin, L.; Guerrero, C.; Abbondanno, U.; Aerts, G.; Álvarez, H.; Álvarez-Velarde, F.; Andriamonje, S.; et al. ^{197}Au(n, γ) cross section in the resonance region. *Phys. Rev. C* **2010**, *81*, 044616. [CrossRef]
68. Lederer, C.; Colonna, N.; Domingo-Pardo, c.; Gunsing, F.; Käppeler, F.; Massimi, C.; Mengoni, A.; Wallner, A.; Abbondanno, U.; Aerts, G.; et al. ^{197}Au(n, γ) cross section in the unresolve resonance region. *Phys. Rev. C* **2011**, *83*, 034608. [CrossRef]
69. Casanovas-Hoste, A.; Domingo-Pardo, C.; Lerendegui-Marco, J.; Guerrero, C.; Tarifeño-Saldivia, A.; Krtička, M.; Pignatari, M.; Calviño, F.; Schumann, D.; Heinitz, S.; et al. Shedding Light on the Origin of ^{204}Pb, the Heaviest s-Process–Only Isotope in the Solar System. *Phys. Rev. Lett.* **2024**, *133*, 052702. [CrossRef]
70. Casanovas-Hoste, A.; Tarifeño-Saldivia, A.E.; Domingo-Pardo, C.; Calviño, F.; Maugeri, E.; Guerrero, C.; Lerendegui-Marco, J.; Dressler, R.; Heinitz, S.; Schumann, D.; et al. Neutron capture measurement at the n_TOF facility of the ^{204}Tl and ^{205}Tl s-process branching points. *J. Phys. Conf. Ser.* **2020**, *1668*, 012005. [CrossRef]
71. Domingo-Pardo, C.; Abbondanno, U.; Aerts, G.; Álvarez-Pol, H.; Alvarez-Velarde, F.; Andriamonje, S.; Andrzejewski, J.; Assimakopoulos, P.; Audouin, L.; Badurek, G.; et al. Measurement of the neutron capture cross section of the s-only isotope ^{204}Pb from 1 eV to 440 keV. *Phys. Rev. C* **2007**, *76*, 015806. [CrossRef]
72. Domingo-Pardo, C.; Abbondanno, U.; Aerts, G.; Álvarez-Pol, H.; Alvarez-Velarde, F.; Andriamonje, S.; Andrzejewski, J.; Assimakopoulos, P.; Audouin, L.; Badurek, G.; et al. Measurement of the radiative neutron capture cross section of ^{206}Pb and its astrophysical implications. *Phys. Rev. C* **2007**, *76*, 045805. [CrossRef]
73. Domingo-Pardo, C.; Abbondanno, U.; Aerts, G.; Álvarez-Pol, H.; Alvarez-Velarde, F.; Andriamonje, S.; Andrzejewski, J.; Assimakopoulos, P.; Audouin, L.; Badurek, G.; et al. Resonance capture cross section of ^{207}Pb. *Phys. Rev. C* **2006**, *74*, 055802. [CrossRef]
74. Domingo-Pardo, C.; Abbondanno, U.; Aerts, G.; Álvarez-Pol, H.; Alvarez-Velarde, F.; Andriamonje, S.; Andrzejewski, J.; Assimakopoulos, P.; Audouin, L.; Badurek, G.; et al. New measurement of neutron capture resonances in ^{209}Bi. *Phys. Rev. C* **2006**, *74*, 025807. [CrossRef]
75. Damone, L.; Barbagallo, M.; Mastromarco, M.; Mengoni, A.; Cosentino, L.; Maugeri, E.; Heinitz, S.; Schumann, D.; Dressler, R.; Käppeler, F.; et al. ^{7}Be(n, p)^{7}Li Reaction and the Cosmological Lithium Problem: Measurement of the Cross Section in a Wide Energy Range at n_TOF at CERN. *Phys. Rev. Lett.* **2018**, *121*, 042701. [CrossRef] [PubMed]
76. Torres-Sánchez, P.; Praena, J.; Porras, I.; Sabaté-Gilarte, M.; Lederer-Woods, C.; Aberle, O.; Alcayne, V.; Amaducci, S.; Andrzejewski, J.; Audouin, L.; et al. Measurement of the ^{14}N(n, p)^{14}C cross section at the CERN n_TOF facility from subthermal energy to 800 keV. *Phys. Rev. C* **2023**, *107*, 064617. [CrossRef]
77. Lederer-Woods, C.; Woods, P.J.; Davinson, T.; Kahl, D.; Lonsdale, S.J.; Aberle, O.; Amaducci, S.; Andrzejewski, J.; Audouin, L.; Bacak, M.; et al. Destruction of the cosmic γ-ray emitter ^{26}Al in massive stars: Study of the key ^{26}Al(n, p) reaction. *Phys. Rev. C* **2021**, *104*, L022803. [CrossRef]
78. Lederer-Woods, C.; Friedman, M.; Battino, U.; Köster, U.; Maugeri, E.; Bacak, M.; Mengoni, A.; Cocolios, T.E.; Cristallo, S.; Davinson, T.; et al. Measurement of ^{40}K(n, p) and ^{40}K(n, α) Cross Sections at n_TOF EAR-2, CERN-INTC-2022-047; INTC-P-645. Available online: http://cds.cern.ch/record/2834656 (accessed on 19 September 2025).
79. Barbagallo, M.; Musumarra, A.; Cosentino, L.; Maugeri, E.; Heinitz, S.; Mengoni, A.; Dressler, R.; Schumann, D.; Käppeler, F.; Colonna, N.; et al. ^{7}Be(n, α)^{4}He Reaction and the Cosmological Lithium Problem: Measurement of the Cross Section in a Wide Energy Range at n_TOF at CERN. *Phys. Rev. Lett.* **2016**, *117*, 152701. [CrossRef]
80. Lederer-Woods, C.; Woods, P.J.; Davinson, T.; Estrade1, A.; Heyse, J.; Kahl, D.; Lonsdale, S.J.; Paradela, C.; Schillebeeckx, P.; Aberle, O.; et al. Destruction of the cosmic γ-ray emitter ^{26}Al in massive stars: Study of the key ^{26}Al(n, α) reaction. *Phys. Rev. C* **2021**, *104*, L032803. [CrossRef]
81. Infantes, F.G.; Lederer-Woods, C.; Battino, U.; Birincioglu, S.; Davinson, T.; Heyse, J.; Manna, A.; Mengoni, A.; Odusina, E.; Paradela, C.; et al. Measurement of ^{41}Ca(n, α) cross sections at n_TOF EAR-2 Relevant to Ca-41 Abundances in the Early Solar System, CERN-INTC-2025-029; INTC-P-741. Available online: https://cds.cern.ch/record/2929624 (accessed on 19 September 2025).
82. Rubbia, C.; Andriamonje, S.; Bouvet-Bensimon, D.; Buono, S.; Cappi, R.; Cennini, P.; Gelès, C.; Goulas, I.; Kadi, Y.; Pavlopoulos, P.; et al. CERN-LHC-98-002-EET—Addendum. 1998. Available online: https://cds.cern.ch/record/363828 (accessed on 19 September 2025).
83. Mengoni, A.; Milazzo, P.M.; Patronis, N. n_TOF at CERN: Status and Perspectives. *Nucl. Phys. News* **2024**, *34*, 26. [CrossRef]
84. Guerrero, C.; Tsinganis, A.; Berthoumieux, E.; Barbagallo, M.; Belloni, F.; Gunsing, F.; Weiss, C.; Chiaveri, C.; Calviani, M.; Vlachoudis, V.; et al. Performance of the neutron time-of-flight facility n_TOF at CERN. *Eur. Phys. J. A* **2013**, *49*, 27. [CrossRef]
85. Weiss, C.; Chiaveri, E.; Girod, S.; Vlachoudis, V.; Aberle, O.; Barros, S.; Bergström, I.; Berthoumieux, E.; Calviani, M.; Guerrero, C.; et al. The new vertical neutron beam line at the CERN n_TOF facility design and outlook on the performance. *Nucl. Instr. Meth. Phys. Res. A* **2015**, *799*, 90. [CrossRef]

86. Patronis, N.; Mengoni, A.; Colonna, N.; Cecchetto, M.; Lerendegui-Marco, J. Aberle, O.; Domingo-Pardo, C.; Gervino, G.; Stamati, M.E.; Goula, S.; et al. The CERN n_TOF NEAR station for astrophysics and application-related neutron activation measurements. *Eur. Phys. J. A* **2025**, *61*, 215.
87. Plag, R.; Heil, M.; Käppeler, F.; Pavlopoulos, P.; Reifarth, R.; Wisshak, K. An optimized C_6D_6 detector for studies of resonance-dominated (n, γ) cross-sections. *Nucl. Instr. Meth. Phys. Res. A* **2003**, *496*, 425. [CrossRef]
88. Mastinu, P.F.; Baccomi, R.; Berthoumieux, E.; Cano-Ott, D.; Gramegna, F.; Guerrero, C.; Massimi, C.; Milazzo, P.M.; Mingrone, F.; Praena, J.; et al. New C_6D_6 Detectors: Reduced Neutron Sensitivity and Improved Safety. Available online: https://cds.cern.ch/record/1558147 (accessed on 19 September 2025).
89. Borella, A.; Aerts, G.; Gunsing, F.; Moxon, W.; Schillebeeckx, P.; Wynants, R. The use of C_6D_6 detectors for neutron induced capture cross-section measurements in the resonance region. *Nucl. Instr. Meth. Phys. Res.A* **2007**, *577*, 626. [CrossRef]
90. Corvi, F.; Prevignano, A.; Liskien, H.; Smith, P.B. An experimental method for determining the total efficiency and the response function of a gamma-ray detector in the range 0.5–10 MeV. *Nucl. Instr. Meth. Phys. Res. A* **1988**, *263*, 475. [CrossRef]
91. Abbondanno, U.; Aerts, G.; Alvarez, H.; Andriamonje, S.; Angelopoulos, A.; Assimakopoulos, P.; Bacri, C.O.; Badurek, G.; Baumann, P.; Bečvář, F.; et al. New experimental validation of the pulse height weighting technique for capture cross-section measurements. *Nucl. Instr. Meth. Phys. Res. A* **2004**, *263*, 454. [CrossRef]
92. Alcayne, V.; Cano-Ott, D.; Garcia, J.; González-Romero, E.; Martínez, T.; Pérez de Rada, A.; Plaza, J.; Sánchez-Caballero, A.; Balibrea-Correa, J.; Domingo-Pardo, C.; et al. A Segmented Total Energy Detector (sTED) optimized for (n, γ) cross-section measurements at n_TOF EAR2. *Rad. Phys. Chem.* **2024**, *217*, 111525. [CrossRef]
93. Guerrero, C.; Abbondanno, U.; Aerts, G.; Álvarez, H.; Álvarez-Velarde, F.; Andriamonje, S.; Andrzejewski, J.; Assimakopoulos, P.; Audouin, L.; Badurek, L.; et al. The n_TOF Total Absorption Calorimeter for neutron capture measurements at CERN. *Nucl. Instr. Meth. Phys. Res. A* **2009**, *608*, 424. [CrossRef]
94. Bao, Z.Y.; Beer, H.; Käppeler, F.; Voss, F.; Wisshak, K.; Rauscher, T. Neutron cross sections for nucleosynthesis studies. *Nucl. Data Tables* **2000**, *76*, 70. [CrossRef]
95. Rauscher, T.; Mohr, P.; Dillmann, I.; Plag, R. Opportunities to constrain astrophysical reaction rates for the s-process via determination of the ground-state cross sections. *Astrophys. J.* **2011**, *738*, 143. [CrossRef]
96. Lambert, D.L.; Smith, V.V.; Busso, M.; Gallino, R.; Straniero, O. The Chemical Composition of Red Giants. IV. The Neutron Density at the s-Process Site. *Astrophys. J.* **1995**, *450*, 302. [CrossRef]
97. Lugaro, M.; Tagliente, G.; Karakas, A.I.; Milazzo, P.M.; Käppeler, F.; Davis, A.M.; Savina, M.R. The impact of updated Zr neutron-capture cross sections and new Asymptotic Giant Branch models on our understanding of the s-process and the origin of stardust. *Astrophys. J.* **2014**, *780*, 95. [CrossRef]
98. Lawler, L.J.; Bonvallet, G.; Sneden, C. Experimental Radiative Lifetimes, Branching Fractions, and Oscillator Strengths for La II and a New Determination of the Solar Lanthanum Abundance. *Astrophys. J.* **2001**, *556*, 452. [CrossRef]
99. Straniero, O.; Cristallo, S.; Piersanti, L. Heavy elements in globular clusters: The role of Asymptotic Giant Branch stars. *Astrophys. J.* **2014**, *785*, 77. [CrossRef]
100. Dillmann, I.; Plag, R.; Käppeler, F.; Rauscher, T. Karlsruhe Astrophysical Database of Nucleosynthesis in Stars. Available online: http://www.kadonis.org (accessed on 19 September 2025).
101. Domingo-Pardo, C.; Aberle, O.; Alcayne, V.; Alpar, G.; Al Halabi, M.; Amaducci, S.; Babiano, V.; Bacak, M.; Balibrea-Correa, J.; Bartolomé, J.; et al. Neutron capture measurements for s-process nucleosynthesis. *Eur. Phys. J. A* **2025**, *61*, 105. [CrossRef] [PubMed]
102. Pignatari, M.; Gallino, R.; Heil, M.; Wiescher, M.; Käppeler, F.; Herwig, F.; Bisterzo, S. The weak s-process in massive stars and its dependence on the neutron capture cross sections. *Astrophys. J.* **2010**, *710*, 1557. [CrossRef]
103. Harder, A.; Michaelsen, S.; Jungclaus, A.; Lieb, K.P.; Williams, A.P.; Börner, H.G.; Trautmannsheimer, M. Double neutron capture in ^{62}Ni. *Zeit. Physik A* **1992**, *343*, 7. [CrossRef]
104. Klay, N.; Käppeler, F. β-decay rate of ^{79m}Se and its consequences for the s-process temperature. *Phys. Rev. C* **1988**, *38*, 295. [CrossRef]
105. Lugaro, M.; Davis, A.M.; Gallino, R.; Pellin, M.J.; Straniero, O.; Käppeler, F. Isotopic Compositions of Strontium, Zirconium, Molybdenum, and Barium in Single Presolar SiC Grains and Asymptotic Giant Branch Stars. *Astrophys. J.* **2003**, *593*, 486. [CrossRef]
106. Lerendegui-Marco, J.; Alcayne, V.; Babiano-Suarez, V.; Bacak, M.; Balibrea-Correa, J.; Casanovas, A.; Domingo-Pardo, C.; de la Fuente, G. Gameiro, B.; García-Infantes, F.; et al. Recent highlights and prospects on (n, γ) measurements at the CERN n_TOF facility. *EPJ Web Conf.* **2025**, *329*, 03003 [CrossRef]
107. Lerendegui-Marco, J.; Casanovas, A.; Alcayne, V.; Aberle, O.; Altieri, S.; Amaducci, S.; Andrzejewski, J.; Babiano-Suarez, V.; Bacak, M.; Balibrea, J.; et al. New perspectives for neutron capture measurements in the upgraded CERN-n_TOF Facility. *EPJ Web Conf.* **2023**, *284*, 01028. [CrossRef]

108. Yin, Q.Z.; Aeolus Lee, C.T.; Ott, U. Signatures of the s-Process in Presolar Silicon Carbide Grains: Barium through Hafnium. *Astrophys. J.* **2006**, *647*, 676. [CrossRef]
109. Cristallo, S.; Piersanti, L.; Straniero, O.; Gallino, R.; Domínguez, I.; Abia, C.; Di Rico, G.; Quintini, M.; Bisterzo, S. Evolution, Nucleosynthesis, and Yields of low-mass Asymptotic Giant Branch stars at different metallicities. II. THE FRUITY DATABASE. *Astrophys. J. Suppl.* **2011**, *197*, 17. [CrossRef]
110. Wagemans, J.; Goeminne, G. Experimental determination of the ^{14}N(n, p)^{14}C reaction cross section for thermal neutrons. *Phys. Rev. C* **2000**, *61*, 064601. [CrossRef]
111. Kitahara, R.; Hirota, K.; Ieki, S.; Ino, T.; Iwashita, Y.; Kitaguchi, M.; Koga, J.; Mishima, K.; Morishita, A.; Nagakura, N.; et al. Improved accuracy in the determination of the thermal cross section of ^{14}N(n, p)^{14}C for neutron lifetime measurement. *Prog. Theor. Exp. Phys.* **2019**, *2019*, 093C01. [CrossRef]
112. Best, A.; Rapagnani, D.; Mercogliano, D. The Ongoing Deep Underground Measurement of ^{22}Ne(α,n)^{25}Mg at the Ion Beam Facility of the INFN-LNGS. *Galaxies* **2024**, *12*, 68. [CrossRef]
113. Talwar, R.; Adachi, T.; Berg, G.P.A.; Bin, L.; Bisterzo, S.; Couder, M.; deBoer, R.J.; Fang, X.; Fujita, H. Probing astrophysically important states in the ^{26}Mg nucleus to study neutron sources for the s-process. *Phys. Rev. C* **2016**, *93*, 055803. [CrossRef]
114. Cyburt, R.H.; Fields, B.D.; Olive, K.A.; Yeh, T.H. Big bang nucleosynthesis: Present status. *Rev. Mod. Phys.* **2016**, *88*, 015004. [CrossRef]
115. Fields, B.D.; Olive, K.A. Implications of the non-observation of ^{6}Li in halo stars for the primordial ^{7}Li problem. *J. Cosmol. Astropart. Phys.* **2022**, *2022*, 78. [CrossRef]
116. Cosentino, L.; Musumarra, A.; Barbagallo, M.; Pappalardo, A.; Colonna, N.; Damone, L.; Piscopo, M.; Finocchiaro, P.; Maugeri, E.; Heinitz, S.; et al. Experimental setup and procedure for the measurement of the ^{7}Be(n, α)α reaction at n_TOF. *Nucl. Instr. Meth. Phys. Res. A* **2016**, *380*, 197. [CrossRef]
117. Clayton, D.D. Cosmoradiogenic Chronologies of nucleosynthesis. *Astrophys. J.* **1964**, *139*, 637. [CrossRef]
118. Laird, A.M.; Lugaro, M.; Kankainen, A.; Adsley, P.; Bardayan, D.W.; Brinkman, H.E.; Côté, B.; Deibel, C.M.; Diehl, R.; Hammache, F. Progress on nuclear reaction rates affecting the stellar production of ^{26}Al. *J. Phys. G Nucl. Part. Phys.* **2023**, *50*, 033002. [CrossRef]
119. Iliadis, C.; Champagne, A.; Chieffi, A.; Limongi, M. The effects of Thermonuclear Reaction rate variations on ^{26}Al production in massive stars: A sensitivity study. *Astrophys. J. Suppl. Ser.* **2011**, *193*, 16. [CrossRef]
120. Limongi, M.; Chieffi, A. The Nucleosynthesis of ^{26}Al and ^{60}Fe in Solar Metallicity Stars Extending in Mass from 11 to 120 M_{solar}: The Hydrostatic and Explosive Contributions. *Astrophys. J.* **2006**, *647*, 483–500. [CrossRef]
121. Battino, U.; Lederer-Woods, C.; Pignatari, M.; Soós, B.; Lugaro, M.; Vescovi, D.; Cristallo, S.; Woods, P.J.; Karakas, A. Impact of newly measured ^{26}Al(n, p)^{26}Mg and ^{26}Al(n, α)^{23}Na reaction rates on the nucleosynthesis of ^{26}Al in stars. *Mon. Not. R. Astron. Soc.* **2023**, *520*, 2436–2444. [CrossRef]
122. Ingelbrecht, C.; Moens, A.; Wagemans, J.; Denecke, B.; Altzitzoglou, T.; Johnston, P. An ^{26}Al target for (n, p) and (n, α) cross-section measurements. *Nucl. Instrum. Methods Phys. Res. Sect. A* **2002**, *480*, 114. [CrossRef]
123. Alpar, G.; Anderson, B.; Bacak, M.; Balibrea, J.; Catlett, D.; Charlton, W.; Domingo-Pardo, C.; Flanagan, W.; Kelly, I.; Lederer-Wood, C.; et al. Measurement of the Zirconium-88 Neutron Absorption Cross Section at EAR2, CERN-INTC-2024-011; INTC-P-693. Available online: https://cds.cern.ch/record/2886135 (accessed on 19 September 2025).
124. Beer, H.; Sedyshev, P.V.; Rochow, W.; Mohr, P.; Oberhummer, H. Neutron capture measurements of the noble gas isotopes ^{22}Ne, ^{40}Ar and ^{78,80,84,86}Kr in the keV energy region. *Nucl. Phys. A* **2002**, *705*, 239. [CrossRef]
125. Aberle, O.; Alcayne, V.; Alpar, G.; Al Halabi, M.; Amaducci, S.; Babiano, V.; Bacak, M.; Balibrea-Correa, J.; Bartolomé, J.; Bernardes, A.P.; et al. Neutron Activation Station at the SPS Beam Dump Facility (BDF). Available online: https://cds.cern.ch/record/2913936 (accessed on 19 September 2025).